ACCEPTED FOR PUBLICATION IN ApJ
Preprint typeset using LATEX style emulateapj v. 08/22/09

arXiv:0905.1697v3 [astro-ph.HE] 30 Oct 2009

AN UP-SCATTERED COCOON EMISSION MODEL OF GAMMA-RAY BURST HIGH-ENERGY LAGS

KENJI TOMA[1,2], XUE-FENG WU[1,2,3], PETER MÉSZÁROS[1,2,4]

accepted for publication in ApJ

ABSTRACT

The *Fermi Gamma-ray Space Telescope* recently detected the most energetic gamma-ray burst so far, GRB 080916C, and reported its detailed temporal properties in an extremely broad spectral range: (i) the time-resolved spectra are well described by broken power-law forms over the energy range of 10 keV – 10 GeV, (ii) the high-energy emission (at $\varepsilon > 100$ MeV) is delayed by ≈ 5 s with respect to the $\varepsilon \lesssim 1$ MeV emission, and (iii) the emission onset times shift towards later times in higher energy bands. We show that this behavior of the high-energy emission can be explained by a model in which the prompt emission consists of two components: one is the emission component peaking at $\varepsilon \sim 1$ MeV due to the synchrotron-self-Compton radiation of electrons accelerated in the internal shock of the jet and the other is the component peaking at $\varepsilon \sim 100$ MeV due to up-scattering of the photospheric X-ray emission of the expanding cocoon (i.e., the hot bubble produced by dissipation of the jet energy inside the progenitor star) off the same electrons in the jet. Based on this model, we derive some constraints on the radius of the progenitor star and the total energy and mass of the cocoon of this GRB, which may provide information on the structure of the progenitor star and the physical conditions of the jet propagating in the star. The up-scattered cocoon emission could be important for other Fermi GRBs as well. We discuss some predictions of this model, including a prompt bright optical emission and a soft X-ray excess.

Subject headings: gamma rays: bursts — gamma-rays: theory

1. INTRODUCTION

Gamma-ray bursts (GRBs) were only sparsely observed in the > 100 MeV range, until the *Fermi* satellite was launched on June 11 2008 (Atwood et al. 2009). Now *Fermi* provides extremely broad energy coverage, 8 keV – 300 GeV, with high sensitivity for GRBs, and is accumulating a wealth of new data which open a completely new window on the physics of GRBs. The high-energy temporal and spectral data provided by *Fermi* can severely constrain the physical parameters of the GRB emission region and the circumburst environment, which will lead to a deeper understanding of the central engine and the GRB progenitors, and will also constrain models of high-energy cosmic ray acceleration (for recent reviews, Falcone et al. 2008; Zhang 2007; Mészáros 2006).

The GRB detected by *Fermi* on September 16 2008 (GRB 080916C) shows several important new properties (Abdo et al. 2009):

(i) The time-resolved spectra (with resolution $\sim 5-50$ s) are well fitted by an empirical broken-power-law function (the so-called Band function, Band et al. 1993) from 8 keV up to a photon with energy ≈ 13.2 GeV.

(ii) The $\varepsilon > 100$ MeV emission is not detected together with the first $\varepsilon \lesssim 1$ MeV pulse and the onset of the $\varepsilon > 100$ MeV emission coincides with the rise of the second pulse (≈ 5 s after the trigger).

(iii) Most of the emission in the second pulse shifts towards later times as higher energies are considered.

(iv) The $\varepsilon > 100$ MeV emission lasts at least 1400 s, while photons with $\varepsilon < 100$ MeV are not detected past 200 s.

(v) The redshift $z \simeq 4.35$ (Greiner et al. 2009) and the fluence $\approx 2.4 \times 10^{-4}$ erg cm^{-2} in the 10 keV - 10 GeV range mean that this is the largest reported isotropic γ-ray energy release, $E_{\gamma,\rm iso} \simeq 8.8 \times 10^{54}$ erg.

Some other bursts detected by the LAT detector of *Fermi* also display high-energy lags, similar to the properties (ii) and/or (iii) (Abdo et al. 2009), and then they should be very important to understand the prompt emission mechanism of GRBs. We will call the $\varepsilon \lesssim 1$ MeV emission and the $\varepsilon > 100$ MeV emission "MeV emission" and "high-energy emission", respectively.

A simple physical picture for the property (i) is that the prompt emission consists of a single emission component, such as synchrotron radiation of electrons accelerated in internal shocks of a relativistic jet. In this picture, the peak of the MeV pulse could be attributed to the cessation of the emission production (i.e., the shock crossing of the shell) and the subsequent emission could come from the high latitude regions of the shell (e.g., Dermer 2004; Zhang et al. 2006). Thus the observed high-energy lag for the second pulse (property (iii)) requires that the electron energy spectrum should be harder systematically in the higher latitude region. This would imply that the particle acceleration process should definitely depend on the global parameters of the jet, e.g., the angle-dependent relative Lorentz factor of the colliding shells, but such a theory has not been formulated yet. The property (ii) could be just due to the fact that the two pulses originate in two internal shocks with different physical conditions for which the electron energy spectrum of the second internal shock is harder than that of the first one (Abdo et al. 2009).

Another picture is that the prompt emission consists of the MeV component and a delayed high-energy component. The latter component could be produced by hadronic effects (i.e.,

Electronic address: toma@astro.psu.edu
[1] Department of Astronomy and Astrophysics, Pennsylvania State University, 525 Davey Lab, University Park, PA 16802, USA
[2] Center for Particle Astrophysics, Pennsylvania State University
[3] Purple Mountain Observatory, Chinese Academy of Sciences, Nanjing 210008, China
[4] Department of Physics, Pennsylvania State University

photo-pion process and proton synchrotron emission) (e.g., Dermer 2002; Asano et al. 2009), because the acceleration of protons or ions to high energies may be delayed behind the electron acceleration. However, it is not clear that hadronic effects can reproduce the smooth Band spectrum (see also Wang et al. 2009).

In this paper, we discuss a different two-component emission picture in which the delayed high-energy component is produced by leptonic process (i.e., electron inverse Compton scattering) [5]. We focus on the effect that the ambient radiation up-scattered by the accelerated electrons in the jet can have a later peak than that of the synchrotron and synchrotron-self-Compton (SSC) emission of the same electrons (corresponding to the property (iii)) (Wang & Mészáros 2006; Fan et al. 2008; Beloborodov 2005). Provided that the seed photons for the Compton scattering come from the region behind the electron acceleration region of the jet (see Figure 1), the up-scattered high-energy photon field is highly anisotropic in the comoving frame of the jet, i.e., the emissivity is much larger for the head-on collisions of the electrons and the seed photons. As a result, a stronger emission is observed from the higher latitude regions, and thus its flux peak lags behind the synchrotron and SSC emission.

Here we propose that the seed photons may be provided by the photospheric emission of an expanding cocoon. GRB 080916C is a long GRB, and it may originate from the collapse of a massive star. The relativistic jet produced in the central region penetrates the star and deposits most of its energy output into a thermal bubble, or cocoon, until it breaks out of the star (e.g., Mészáros & Rees 2001; Zhang et al. 2003; Mizuta et al. 2006). The cocoon can store an energy comparable or larger than the energy of the prompt emission of the jet, and thus it may make an observable signature outside the star (Ramirez-Ruiz et al. 2002; Pe'er et al. 2006). The cocoon escaping from the star will emit soft X-rays, and these can be up-scattered by the accelerated electrons in the jet into the high-energy range. The optical thinning of the expanding cocoon may be delayed behind the prompt emission of the jet, so that the onset of the high-energy emission is delayed behind the MeV emission (corresponding to the property (ii)). Thus this model has the potential for explaining the two delay timescales; the delayed onset of the high-energy photons (property (ii)) is due to the delayed emission of the cocoon, while the high-energy lag within the second pulse (property (iii)) is due to the anisotropic inverse Compton scattering. We also show that the combination of the time-averaged spectra of the SSC and the up-scattered cocoon (UC) emission is roughly consistent with the observed smooth power-law spectrum (property (i)) (see Figure 2).

As we will explain below, the UC emission is short-lived and may not account for the whole high-energy emission, which lasts much longer than the MeV emission (property (iv)). It is natural that the high-energy emission in later times is related to the afterglow, i.e., produced by the external shock which propagates in the circumburst medium. This possibility is studied by Kumar & Barniol Duran (2009). They claim that even the onset phase of the high-energy emission is produced by the external shock. However, the rise of the flux of GRB 080916C in the LAT energy range ($\sim t^6$) is too steep for the external shock to reproduce it. Thus at least the first part of the delayed high-energy component of this burst should be related to the prompt emission.

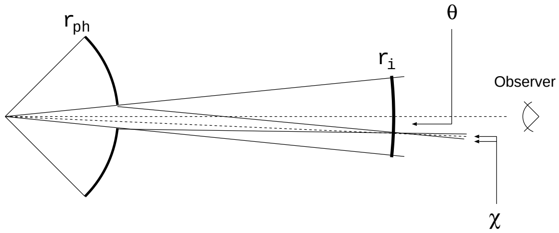

FIG. 1.— Geometry of our model. The jet with opening angle $\theta_j \simeq 0.01$ and the cocoon with opening angle $\theta_c \simeq 0.8$ are ejected from the collapsing star. The cocoon becomes optically thin at $r = r_{\rm ph} \simeq 2.1 \times 10^{14}$ cm $E_{c,52}^{1/2}$ $(\Gamma_c/50)^{-1/2}$ some time ($\lesssim 5$ s) after the burst trigger (see text for detail). The second pulse of the prompt emission is produced by the accelerated electrons in the internal shock of the jet at $r = r_i \simeq 2.2 \times 10^{16}$ cm $\Gamma_{j,3}^2$ $(\Delta t_i/2$ s), and the cocoon X-ray photons are up-scattered by the same electrons at $r = r_i$ into the GeV range. The jet is assumed to be observed from the direction of the jet axis, and θ describes the emitting point of the high-latitude emission. The angle χ describes the difference of the directions of the expansion and the cocoon photon beams, which can be neglected for our adopted parameters.

Although some *Fermi*-LAT GRBs show high-energy lags, the observational analysis of the delayed high-energy emission is fairly complete only for GRB 080916C at the moment, and its data is quite extensive. Thus we focus on this burst to examine whether the UC emission is viable for its properties in the high energy range in this paper. However, our modeling is generic, and we will show that the UC emission could be important for some other *Fermi*-LAT GRBs (including short GRBs).

This paper is organized as follows. In § 2, we derive the delay time of the onset of the cocoon photospheric emission behind the MeV pulse of the jet, and calculate the flux of the cocoon emission. In § 3, we constrain the physical conditions of the emitting region of the jet by assuming that the MeV emission is due to the 1st-order SSC radiation, and show that the UC flux of the jet and its lag timescale are compatible with the observed GeV emission. In § 4, we calculate the spectrum and lightcurve in a simple numerical manner and find appropriate values of the physical parameters of the cocoon and jet for reproducing the observed spectrum at $\varepsilon \gtrsim 1$ MeV and lightcurve of GRB 080916C as the combination of the 1st-order SSC and UC emission. We discuss the emission at $\varepsilon < 1$ MeV and the thermal emission of the jet in § 5. The UC emission for other long and short GRBs are discussed in § 6. We summarize our model and its implications in § 7. We use keV cm^{-2} s^{-1} keV^{-1} and keV cm^{-2} s^{-1} for the units of the flux density and flux, respectively, for comparison with Fermi papers, e.g., Abdo et al. (2009). The conversion factors to usual units are useful: 1 keV cm^{-2} s^{-1} keV^{-1} = 6.63×10^{-27} erg cm^{-2} s^{-1} Hz^{-1} and 1 keV cm^{-2} s^{-1} = 1.60×10^{-9} erg cm^{-2} s^{-1}.

2. COCOON DYNAMICS

The dynamics of the cocoon after escaping from the star is studied in Ramirez-Ruiz et al. (2002) and Pe'er et al. (2006). Based on these studies, we derive the delay time of the cocoon emission behind the prompt emission of the jet and the energy flux of the cocoon emission.

2.1. *Time delay of the cocoon emission onset*

The cocoon dynamics is dominated by its radiation energy while it is inside the star. We take the total energy and the total mass of the cocoon and the stellar radius as parameters, E_c, M_c, and r_*, respectively. After the jet breaks out of the star, the cocoon expands with the sound speed, $c_s = c/\sqrt{3}$, where c is the speed of light. The cocoon expands by its own thermal pressure in the comoving frame as expected in the standard fireball model (Mészáros et al. 1993; Piran et al. 1993). Its expansion speed in the comoving frame suddenly becomes close to c, and then the opening angle of the cocoon measured in the central engine frame is given by $\theta_c \simeq \Gamma_{c,\mathrm{ex}}^{-1}$, where $\Gamma_{c,\mathrm{ex}}$ is the Lorentz factor corresponding to c_s. Thus we obtain $\theta_c \simeq \sqrt{2/3} \simeq 0.8$. Morsony et al. (2007) have performed detailed numerical simulations of the cocoon expansion outside the star, which show that the opening angle of the expanding cocoon is $\sim 40°$. This is consistent with the above analytical estimate.

---

[5] Other ideas for the delayed high-energy emission of GRB 080916C in the leptonic model are proposed in Li (2009), Zou et al. (2009), and Fan (2009) (see also Aoi et al. 2009).

The cocoon material accelerates as $\Gamma \propto r$ and reaches the terminal Lorentz factor $\Gamma_c = E_c/M_c c^2$ at

$$r_s = r_* \Gamma_c = 5.0 \times 10^{12}\ \mathrm{cm}\ r_{*,11} \left(\frac{\Gamma_c}{50}\right). \tag{1}$$

Hereafter we adopt the notation $Q = 10^x Q_x$ in cgs units. For $r > r_s$, the cocoon material is dominated by the kinetic energy. The radiation stored in the cocoon is released when the opacity for the electron scattering becomes less than unity. The photosphere radius is given by

$$r_{\mathrm{ph}} \simeq \left[\frac{E_c \sigma_T}{2\pi(1-\cos\theta_c)\Gamma_c m_p c^2}\right]^{1/2} \simeq 2.1 \times 10^{14}\ \mathrm{cm}\ E_{c,52}^{1/2} \left(\frac{\Gamma_c}{50}\right)^{-1/2}, \tag{2}$$

where σ_T is Thomson cross section.

The cocoon may become optically thin later than the onset of the first MeV pulse (i.e., the burst trigger time). Let $t = 0$ be the photon arrival time at the earth emitted at the stellar surface at the jet breakout. The first MeV pulse produced within the jet at $r = r_i$ is observed at

$$t \simeq \Delta t_i \equiv \frac{r_i}{2c\Gamma_j^2}(1+z), \tag{3}$$

where Γ_j is the bulk Lorentz factor of the jet and z is the source redshift. This timescale is comparable to the angular spreading timescale of the pulse, and we can take $\Delta t_i \simeq 2$ s for GRB 080916C. The second MeV pulse is observed $\simeq 5$ s after the burst trigger, i.e., at $t \simeq \Delta t_i + 5 \simeq 7$ s. On the other hand, the cocoon photospheric emission is observed at

$$t \simeq \Delta t_c \equiv \frac{r_{\mathrm{ph}}}{2c\Gamma_c^2}(1+z) \simeq 7.5\ \mathrm{s}\ E_{c,52}^{1/2} \left(\frac{\Gamma_c}{50}\right)^{-5/2}, \tag{4}$$

where we have used $z \simeq 4.35$. The cocoon photospheric emission may be observed from $t = \Delta t_c$ to $t = \Delta t_c + \Delta t_d$, where $\Delta t_d \sim \Delta t_c$ is the time during which the cocoon will be adiabatically cooled. If internal dissipation occurs in the jet at $r = r_i > r_{\mathrm{ph}}$ making the second MeV pulse within the duration of the cocoon emission, the cocoon photons may be upscattered to higher energies by the energetic electrons within the dissipation region of the jet, which may be observed along with the second MeV pulse. Therefore we require a condition $\Delta t_i < \Delta t_c \lesssim \Delta t_i + 5$. This condition puts a constraint to the physical parameters of the cocoon,

$$0.3 < E_{c,52}^{1/2} \left(\frac{\Gamma_c}{50}\right)^{-5/2} \lesssim 0.9 \tag{5}$$

We adopt the parameters $E_c \simeq 10^{52}$ erg and $\Gamma_c \simeq 50$ for the purposes of calculating the flux of the cocoon emission.

2.2. *Flux of the cocoon emission*

The kinetic energy of the cocoon can be dissipated into radiation energy, e.g., via internal shocks or magnetic reconnection during the expansion. Since the cocoon material may initially have some inhomogeneities caused by the interaction with the jet and the stellar envelope, on scales $\sim \alpha r_*$, where $\alpha \leq 1$ is a numerical factor, internal shocks may occur at (Rees & Mészáros 1994; Mészáros & Rees 2000)

$$r_d \simeq 2\alpha r_* \Gamma_c^2 \simeq 5.0 \times 10^{13}\ \mathrm{cm}\ r_{*,11} \left(\frac{\Gamma_c}{50}\right)^2 \left(\frac{\alpha}{0.1}\right). \tag{6}$$

We focus on the case of $r_s < r_d < r_{\mathrm{ph}}$, in which the optical depth for the electron scattering in the dissipation region is large and the photons produced by the dissipation undergo multiple Compton scattering before escape. As a result, the emerging spectrum is expected to be quasi-thermal (Pe'er et al. 2006). The condition $r_s < r_d < r_{\mathrm{ph}}$ reduces, by equations (1), (2), and (5) into

$$0.01 \left(\frac{\Gamma_c}{50}\right)^{-1} < \alpha < 0.4\, r_{*,11}^{-1}. \tag{7}$$

The comoving temperature of the cocoon when its opening angle becomes θ_c is approximately given by [6]

$$T'_{\mathrm{init}} \simeq \left[\frac{E_c}{2\pi(1-\cos\theta_c) r_*^3 a}\right]^{1/4} \simeq 1.6 \times 10^8\ \mathrm{K}\ E_{c,52}^{1/4} r_{*,11}^{-3/4}, \tag{8}$$

where a is the Stefan constant. The comoving temperature evolves adiabatically as $T' \propto r^{-1}$ for $r_* < r < r_s$ (i.e., in the radiation-dominated phase) and $T' \propto r^{-2/3}$ at $r > r_s$ (i.e., in the matter-dominated phase) (Mészáros et al. 1993), and thus the temperature at $r = r_d$ is

$$T'_{ad} = T'_{\mathrm{init}} \left(\frac{r_s}{r_*}\right)^{-1} \left(\frac{r_d}{r_s}\right)^{-2/3}. \tag{9}$$

If the fraction ϵ_d of the kinetic energy is converted into thermal energy at $r = r_d$, the corresponding temperature is

$$T'_d = \left[\frac{E_c \epsilon_d / \Gamma_c}{2\pi(1-\cos\theta_c) r_d^2 r_* \Gamma_c a}\right]^{1/4} = T'_{ad} \left(\frac{r_d}{r_s}\right)^{1/6} \epsilon_d^{1/4}. \tag{10}$$

If the dissipation is not too strong, i.e., $\epsilon_d \lesssim (r_d/r_s)^{-2/3}$, the temperature at $r = r_d$ is given by T'_{ad} (cf. Rees & Mészáros 2005). After the dissipation the temperature evolves as $T' \propto r^{-2/3}$ since the cocoon shell is still dominated by the kinetic energy and the shell spreading effect is negligible up to $r \sim 2r_* \Gamma_c^2 > r_{\mathrm{ph}}$. The comoving temperature at the photosphere radius is then estimated by

$$T'_{\mathrm{ph}} = T'_{ad} \left(\frac{r_{\mathrm{ph}}}{r_d}\right)^{-2/3} \simeq 2.7 \times 10^5\ \mathrm{K}\ E_{c,52}^{-1/12} r_{*,11}^{-1/12}. \tag{11}$$

[6] The initial temperature of the cocoon may be estimated more accurately. The temperature of the cocoon just before the jet break-out is $T'_i = [E_c/(V'_i a)]^{1/4}$, where the volume of the cocoon can be approximated as $V'_i \approx \pi \theta_{ci}^2 r_*^3/3$ (θ_{ci} is the opening angle of the cocoon just before the jet break-out.) The cocoon escapes from the star and its comoving volume is $V'_{\mathrm{init}} \approx 2\pi(1-\cos\theta_c) r_*^3/3$ when the opening angle becomes θ_c. (The relativistic contraction effect is negligible.) At that time the temperature is calculated as $T'_{\mathrm{ex}} \simeq T'_i (V'_{\mathrm{init}}/V'_i)^{-1/3} \simeq 0.93\ T'_{\mathrm{init}} \theta_{ci,-1}^{1/6}$. To simplify the equations in the following, we neglect the weak dependence on θ_{ci} and adopt T'_{init}.

The photospheric emission of the cocoon is expected to have a quasi-thermal spectrum

$$F_\varepsilon^{\rm co} = F_{\varepsilon_{\rm ph}}^{\rm co} \times \begin{cases} \left(\frac{\varepsilon}{\varepsilon_{\rm ph}^{\rm co}}\right)^2 & \text{for } \varepsilon < \varepsilon_{\rm ph}^{\rm co}, \\ \left(\frac{\varepsilon}{\varepsilon_{\rm ph}^{\rm co}}\right)^\beta & \text{for } \varepsilon_{\rm ph}^{\rm co} < \varepsilon < \varepsilon_{\rm cut}^{\rm co}, \end{cases} \tag{12}$$

where $\varepsilon_{\rm ph}^{\rm co}$ and $F_{\varepsilon_{\rm ph}}^{\rm co}$ are given by

$$\varepsilon_{\rm ph}^{\rm co} \simeq 2.82\, kT'_{\rm ph} \frac{2\Gamma_c}{1+z} \simeq 1.2 \text{ keV } E_{c,52}^{-1/12} r_{*,11}^{-1/12} \left(\frac{\Gamma_c}{50}\right) \tag{13}$$

$$F_{\varepsilon_{\rm ph}}^{\rm co} \simeq \frac{(1+z)^3}{d_L^2} \frac{2\pi(\nu_{\rm ph}^{\rm co})^2}{c^2} kT'_{\rm ph}\Gamma_c \left(\frac{r_{\rm ph}}{\Gamma_c}\right)^2$$
$$\simeq 31 \text{ keV cm}^{-2} \text{ s}^{-1} \text{ keV}^{-1}\, E_{c,52}^{3/4} r_{*,11}^{-1/4}, \tag{14}$$

where $\nu_{\rm ph}^{\rm co} = \varepsilon_{\rm ph}^{\rm co}/h$ (h is the Planck constant), and we have taken the luminosity distance of GRB 080916C as $d_L \simeq 1.2 \times 10^{29}$ cm. These are derived by assuming that the cocoon is viewed on-axis, and this assumption is validated in § 3.1. Pe'er et al. (2006) carried out detailed numerical calculations of the radiative processes in the cocoon and show that the cocoon photospheric emission has the above spectral form, with $\beta \sim -1$ regardless of the dissipation process if $r_d < r_{\rm ph}$. The cutoff energy $\varepsilon_{\rm cut}^{\rm co}$ is given by $\sim 30 \times \varepsilon_{\rm ph}^{\rm co}$.

The observation of GRB 080916C shows that there is no excess from the Band spectrum at the X-ray band, $\gtrsim 10$ keV, and we obtain a rough upper limit of the cocoon X-ray emission $\varepsilon_{\rm ph}^{\rm co} F_{\varepsilon_{\rm ph}}^{\rm co} \lesssim 40$ keV cm^{-2} s^{-1}. This limit leads to another constraint on the cocoon parameters,

$$r_{*,11} \gtrsim 0.8\, E_{c,52}^2 \left(\frac{\Gamma_c}{50}\right)^3. \tag{15}$$

3. UP-SCATTERED COCOON (UC), SYNCHROTRON, AND SSC EMISSION

We describe here the calculations of the fluxes of the UC, synchrotron, and SSC emission of the jet for the second pulse of GRB 080916C in the internal shock model. The *Fermi* observation allows us to constrain some global parameters of the jet (§ 3.1), and we show that the 1st-order SSC radiation of electrons accelerated in an internal shock can explain the peak energy and the peak flux of the MeV emission (§ 3.2). Then we show that the same electrons can produce the UC emission which lags behind the SSC emission and has the peak energy and the peak flux compatible with the observation in the GeV range (§ 3.3).

3.1. *Overall properties of the jet*

We can constrain, from the *Fermi* observation, the global physical parameters of the jet: the bulk Lorentz factor Γ_j, the emission radius of the second pulse r_i, and the opening angle θ_j. First of all, from the absence of a $\gamma\gamma$ absorption cutoff, we obtain a lower limit on the bulk Lorentz factor of the jet, $\Gamma_j \gtrsim 870$ (Abdo et al. 2009). Since the angular spreading timescale of the pulse is $\Delta t_i \simeq 2$ s for the second pulse, similar to the first pulse, the emission radius is estimated by

$$r_i \simeq 2c\Gamma_j^2 \frac{\Delta t_i}{1+z} \simeq 2.2 \times 10^{16} \text{ cm } \Gamma_{j,3}^2 \left(\frac{\Delta t}{2 \text{ s}}\right). \tag{16}$$

Since GRB 080916C is so bright, it is probable that the jet is viewed on-axis, and we adopt this assumption as a simplification (see Figure 1). In this case, the cocoon is viewed off-axis, since the jet cone will not be filled with the cocoon material. The cocoon emission is thus less beamed, but this off-axis effect is not significant because the opening angle of the jet can be estimated to be small. The isotropic γ-ray energy of this burst is 8.8×10^{54} erg. To obtain a realistic value of the collimation-corrected γ-ray energy, $\lesssim 10^{51}$ erg, the jet opening angle is constrained by $\theta_j \lesssim 0.015$. We adopt $\theta_j \simeq 0.01$, and having adopted a nominal value of $\Gamma_c \simeq 50$ in accord with the observed time delay of the high-energy emission (equation 5), we obtain

$$\Gamma_c\theta_j \simeq 0.5 < 1. \tag{17}$$

Thus the off-axis dimming and softening effects are not significant for the cocoon emission.

3.2. *Internal shock model for the MeV emission*

We assume that the jet is dominated by the kinetic energy of protons (instead of magnetic energy) and we estimate the physical parameters of the jet dissipation region for the second MeV pulse. In the scenario where the dissipation is due to internal shocks (Rees & Mészáros 1994) (see also Panaitescu & Mészáros 2000; Guetta & Granot 2003; Gupta & Zhang 2007; Kumar & McMahon 2008; Bosnjak et al. 2009), the collisionless shock waves can amplify the magnetic field and accelerate electrons to a power-law energy distribution, which then produce synchrotron radiation and SSC radiation. We find that the 1st-order SSC radiation can account for the observed MeV emission. At $r = r_i$, the comoving number density of the jet is estimated by

$$n' = \frac{L\Delta t_i/(1+z)}{4\pi r_i^3 m_p c^2} = \frac{L(1+z)^2}{32\pi m_p c^5 \Gamma_j^6 \Delta t_i^2}$$
$$\simeq 1.7 \times 10^7 \text{ cm}^{-3}\, L_{55}\Gamma_{j,3}^{-6} \left(\frac{\Delta t_i}{2 \text{ s}}\right)^{-2}, \tag{18}$$

where L is the isotropic-equivalent luminosity of the jet, and we have used the fact that the dynamical timescale of the emitting shell measured in the central engine frame is comparable to the angular spreading timescale given by $\Delta t_i/(1+z)$. The optical depth of the electron scattering is calculated as

$$\tau = \sigma_T n' \frac{r_i}{\Gamma_j} \simeq 2.6 \times 10^{-4}\, L_{55}\Gamma_{j,3}^{-5} \left(\frac{\Delta t_i}{2 \text{ s}}\right)^{-1}. \tag{19}$$

This indicates that the dissipation region is optically thin, which allows the non-thermal synchrotron and SSC emission to be observed.

The internal energy density produced by the internal shock is given by $u' = n'\theta_p m_p c^2$, where θ_p is a mean random Lorentz factor of the shocked protons and it is of order unity. Assuming that a fraction ϵ_B of the internal energy of the protons is carried into the magnetic field, the field strength is estimated by

$$B' = (8\pi\epsilon_B u')^{1/2} \simeq 2.6 \text{ G } L_{55}^{1/2}\Gamma_{j,3}^{-3} \left(\frac{\Delta t_i}{2 \text{ s}}\right)^{-1} \theta_p^{1/2} \left(\frac{\epsilon_B}{10^{-5}}\right)^{1/2}. \tag{20}$$

Assuming that a fraction ϵ_e of the internal energy of the protons is given to the electrons, the minimum Lorentz factor of the electrons is given by

$$\gamma_m = \frac{p-2}{p-1}\frac{m_p}{m_e}\epsilon_e\theta_p \simeq 400\,\theta_p\left(\frac{\epsilon_e}{0.4}\right), \tag{21}$$

where p is the index of the electron energy distribution and we have assumed $p \simeq 3.2$ (see § 4 for this number). We find that the electrons are radiatively cooled significantly within the dynamical time for the parameters for fitting the observational data (see § 4), and the electron energy spectrum averaged over the dynamical time is expected to be

$$N'(\gamma) \propto \begin{cases} \gamma^{-2} & \text{for } \gamma_c < \gamma < \gamma_m, \\ \gamma^{-p-1} & \text{for } \gamma_m < \gamma, \end{cases} \tag{22}$$

where γ_c is the cooling Lorentz factor of the electrons, estimated by

$$\gamma_c = \frac{6\pi m_e c}{\sigma_T B'^2(1+x_1+x_1 x_{\rm uc})r_i/(c\Gamma_j)}. \tag{23}$$

Here x_1 and $x_{\rm uc}$ are the luminosity ratios of the 1st-order SSC radiation to the synchrotron radiation and the UC radiation to the 1st-order SSC radiation, respectively. The 2nd-order SSC radiation luminosity is negligible compared to the 1st-order SSC radiation because of the Klein-Nishina suppression. Since x_1 and $x_{\rm uc}$ are complicated functions of γ_c, one cannot obtain a simple analytical formula for estimating γ_c, but we can estimate γ_c for the purpose of fitting the data of GRB 080916C in this model. We find $\gamma_c \sim \gamma_m$ for fitting the observational data (see § 4), and thus the parameter x_1 is written as

$$x_1 = \frac{4}{3}\tau\gamma_c^2\frac{p}{p-2}. \tag{24}$$

We find that $x_{\rm uc} \sim 0.5$ in order for the UC emission flux to be compatible with the observed flux in the GeV range, and thus equation (23) and (24) lead to a formula for estimating the cooling Lorentz factor,

$$\gamma_c \simeq 360\left(\frac{\epsilon_B}{10^{-5}}\right)^{-1/3}\left(\frac{\tau}{4\times10^{-4}}\right)^{-2/3}. \tag{25}$$

The synchrotron characteristic energy and the synchrotron peak flux (at the synchrotron energy corresponding to γ_c) are estimated by

$$\begin{aligned}\varepsilon_m &\simeq \frac{3heB'}{4\pi m_e c}\gamma_m^2\frac{2\Gamma_j}{1+z} \\ &\simeq 2.7\ {\rm eV}\ L_{55}^{1/2}\Gamma_{j,3}^{-2}\left(\frac{\Delta t_i}{2\ {\rm s}}\right)^{-1}\theta_p^{5/2}\left(\frac{\epsilon_B}{10^{-5}}\right)^{1/2}\left(\frac{\epsilon_e}{0.4}\right)^2,\end{aligned} \tag{26}$$

$$\begin{aligned}F_{\varepsilon_c} &\simeq \frac{\sqrt{3}e^3B'N}{m_e c^2}\frac{2\Gamma_j(1+z)}{4\pi d_L^2} \\ &\simeq 1.3\times10^4\ {\rm keV\ cm^{-2}\ s^{-1}\ keV^{-1}}\ L_{55}^{3/2}\Gamma_{j,3}^{-3}\theta_p^{1/2}\left(\frac{\epsilon_B}{10^{-5}}\right)^{1/2},\end{aligned} \tag{27}$$

where $N = [L\Delta t_i/(1+z)]/(\Gamma_j m_p c^2)$. The 1st-order SSC characteristic energy and the SSC peak flux are approximately

$$\begin{aligned}\varepsilon_m^{\rm SC} &\simeq 4\gamma_m^2\varepsilon_m \\ &\simeq 1.7\ {\rm MeV}\ L_{55}^{1/2}\Gamma_{j,3}^{-2}\left(\frac{\Delta t_i}{2\ {\rm s}}\right)^{-1}\theta_p^{9/2}\left(\frac{\epsilon_B}{10^{-5}}\right)^{1/2}\left(\frac{\epsilon_e}{0.4}\right)^4,\end{aligned} \tag{28}$$

$$\begin{aligned}F_{\varepsilon_c}^{\rm SC} &\simeq \tau F_{\varepsilon_c} \\ &\simeq 3.4\ {\rm keV\ cm^{-2}\ s^{-1}\ keV^{-1}}\ L_{55}^{5/2}\Gamma_{j,3}^{-8}\left(\frac{\Delta t_i}{2\ {\rm s}}\right)^{-1}\theta_p^{1/2}\left(\frac{\epsilon_B}{10^{-5}}\right)^{1/2}\end{aligned} \tag{29}$$

The synchrotron self-absorption optical depth at $\varepsilon < \varepsilon_c \equiv \varepsilon_m(\gamma_c/\gamma_m)^2$ can be estimated by (Matsumiya & Ioka 2003; Toma et al. 2008)

$$\tau_a \simeq \frac{2\pi^2(p+3)p}{9\Gamma_E(\frac{1}{3})(p+\frac{5}{3})}\frac{e}{\sigma_T}\tau B'^{-1}\gamma_c^{-5}\left(\frac{\varepsilon}{\varepsilon_c}\right)^{-5/3}, \tag{30}$$

where $\Gamma_E(x)$ is the Euler's Gamma function and we have assumed that $\gamma_c \sim \gamma_m$. Then the ratio of the frequency at which $\tau_a = 1$ to ε_c is given by

$$\frac{\varepsilon_a}{\varepsilon_c} \simeq 0.20\,L_{55}^{3/10}\Gamma_{j,3}^{-6/5}\theta_p^{-3/10}\left(\frac{\epsilon_B}{10^{-5}}\right)^{-3/10}\left(\frac{\gamma_c}{400}\right)^{-3}. \tag{31}$$

The spectrum of the 1st-order SSC emission is described by

$$F_\varepsilon \simeq F_{\varepsilon_c}^{\rm SC}\times\begin{cases}\left(\frac{\varepsilon_a^{\rm SC}}{\varepsilon_c^{\rm SC}}\right)^{1/3}\left(\frac{\varepsilon}{\varepsilon_a^{\rm SC}}\right)^{1}, & \text{for } \varepsilon < \varepsilon_a^{\rm SC}, \\ \left(\frac{\varepsilon}{\varepsilon_c^{\rm SC}}\right)^{1/3}, & \text{for } \varepsilon_a^{\rm SC} < \varepsilon < \varepsilon_c^{\rm SC}, \\ \left(\frac{\varepsilon}{\varepsilon_c^{\rm SC}}\right)^{-1/2}, & \text{for } \varepsilon_c^{\rm SC} < \varepsilon < \varepsilon_m^{\rm SC}, \\ \left(\frac{\varepsilon_m^{\rm SC}}{\varepsilon_c^{\rm SC}}\right)^{-1/2}\left(\frac{\varepsilon}{\varepsilon_m^{\rm SC}}\right)^{-p/2}, & \text{for } \varepsilon_m^{\rm SC} < \varepsilon,\end{cases} \tag{32}$$

where

$$\varepsilon_a^{\rm SC} = 4\gamma_c^2\varepsilon_a,\ \ \varepsilon_c^{\rm SC} = 4\gamma_c^2\varepsilon_c. \tag{33}$$

The $\varepsilon F_\varepsilon$ peak energy is given by $\varepsilon_m^{\rm SC}$. Equation (28) and (29) imply that the 1st-order SSC radiation can explain the flux of the observed MeV emission.

The 2nd-order SSC emission is significantly suppressed by the Klein-Nishina effect. The peak of the 2nd-order SSC spectrum is given by

$$\varepsilon_{\rm KN} = \Gamma_j\gamma_c m_e c^2\frac{1}{1+z} \simeq 38\ {\rm GeV}\ \Gamma_{j,3}\left(\frac{\gamma_c}{400}\right). \tag{34}$$

3.3. *Spectral and temporal behavior of the UC emission*

Here we derive the observed spectrum of the UC emission as a function of the polar angle θ of the emitting region on the shell (see Figure 1). In the comoving frame of the jet, the seed cocoon photons are highly anisotropic. As a result, the cocoon photons up-scattered by isotropic electrons have an anisotropic energy distribution. The spectrum of radiation scattered at an angle $\theta'_{\rm sc}$ relative to the direction of the photon beam in the Thomson scattering regime is given by (Aharonian & Atoyan 1981; Brunetti 2001; Wang & Mészáros 2006; Fan et al. 2008)

$$j'_{\varepsilon'}(\theta'_{\rm sc}) = \frac{3}{2}\sigma_T(1-\cos\theta'_{\rm sc})\int d\gamma N'(\gamma)\int_0^1 dy J'_{\varepsilon'_s}(1-2y+2y^2), \tag{35}$$

where $y = \varepsilon'/[2\gamma^2\varepsilon'_s(1-\cos\theta'_{\rm sc})]$. This is the scattered radiation emissivity in the jet comoving frame, $N'(\gamma)$ is the electron energy spectrum, given by equation (22), and $J'_{\varepsilon'_s}$ is the intensity of the seed photons averaged over solid angle, i.e., the mean intensity. This equation can be directly derived by averaging equation (17) of Brunetti (2001) over the electron directions. When this equation is averaged over $\cos\theta'_{\rm sc}$, it reduces to the equation for isotropic IC emission (Sari & Esin 2001). The term $\xi \equiv 1-\cos\theta'_{\rm sc}$ describes the anisotropy of the spectrum, and this is due to the fact that the IC scattering is strongest for the head-on collisions between electrons and seed photons. This implies that the UC emission in the observer frame is stronger from the high-latitude region of the shell, so that its flux peak lags behind the onset of the synchrotron and SSC emission of the same electrons, which have isotropic energy distribution in the comoving frame of the jet.

If the direction of the photon beam is identical to the direction of the expansion of the scattering point of the jet, we may take $\theta'_{\rm sc} = \theta'$ to calculate the observed flux from the scattering point with the polar angle θ' with respect to the jet axis measured in the jet comoving frame. In this case

$$\xi \equiv 1-\cos\theta'_{\rm sc} = 1-\cos\theta' \approx \frac{2\Gamma_j^2\theta^2}{1+\Gamma_j^2\theta^2}. \tag{36}$$

In our case, the cocoon is viewed off-axis, and the direction of the seed photon beam in the comoving frame is not identical to that of the expansion (see Figure 1). However, the difference is found to be negligible for our adopted parameters. The angle between the direction of the photon beam and the expansion direction in the lab frame is $\chi \approx (r_{\rm ph}/r_i)(\theta_j-\theta) \sim 10^{-4}$, since we focus on the region of $\theta < \Gamma_j^{-1} \ll \theta_j$. Our case has

$$\xi = 1-\cos(\theta' \pm \chi') \approx \frac{2\Gamma_j^2(\theta\pm\chi)^2}{(1+\Gamma_j^2\theta^2)(1+\Gamma_j^2\chi^2)}. \tag{37}$$

Since $\Gamma_j\chi \sim 0.1$, and thus the difference between the values of ξ for the on-axis and off-axis cases is so small that we can use the on-axis equation (36).

The mean intensity of the cocoon emission measured at $r = r_i$ in the central engine frame is calculated as

$$J_{\varepsilon_s} = \frac{1}{4\pi r_i^2}\frac{d_L^2}{1+z}F_{\varepsilon_s}^{\rm co}, \tag{38}$$

and $J'_{\varepsilon'_s} = J_{\varepsilon_s}/(2\Gamma_j)$. We perform the integration in equation (35) approximately and obtain an analytical form

$$j'_{\varepsilon'}(\theta') \simeq \frac{3}{2}\sigma_T\xi(\theta')n'J'_{\varepsilon'_{\rm ph}}g(\varepsilon'), \tag{39}$$

where

$$J'_{\varepsilon'_{\rm ph}} = \frac{1}{4\pi r_i^2}\frac{d_L^2}{1+z}\frac{F_{\varepsilon_{\rm ph}}^{\rm co}}{2\Gamma_j}, \tag{40}$$

$$g(\varepsilon') = \begin{cases} \left(\frac{\varepsilon'}{\varepsilon_c^{\rm UC\prime}}\right)^{1}, & \text{for } \varepsilon' < \varepsilon_c^{\rm UC\prime}, \\ \left(\frac{\varepsilon'}{\varepsilon_c^{\rm UC\prime}}\right)^{-1/2}, & \text{for } \varepsilon_c^{\rm UC\prime} < \varepsilon' < \varepsilon_m^{\rm UC\prime}, \\ \left(\frac{\varepsilon_m^{\rm UC\prime}}{\varepsilon_c^{\rm UC\prime}}\right)^{-1/2}\left(\frac{\varepsilon'}{\varepsilon_m^{\rm UC\prime}}\right)^{\beta}, & \text{for } \varepsilon_m^{\rm UC\prime} < \varepsilon' < \varepsilon_{\rm cut}^{\rm UC\prime}, \\ \left(\frac{\varepsilon_m^{\rm UC\prime}}{\varepsilon_c^{\rm UC\prime}}\right)^{-1/2}\left(\frac{\varepsilon_{\rm cut}^{\rm UC\prime}}{\varepsilon_m^{\rm UC\prime}}\right)^{\beta}\left(\frac{\varepsilon'}{\varepsilon_{\rm cut}^{\rm UC\prime}}\right)^{-p/2}, & \text{for } \varepsilon_{\rm cut}^{\rm UC\prime} < \varepsilon'. \end{cases} \tag{41}$$

Here we define

$$\varepsilon_c^{\rm UC\prime} = 2\gamma_c^2\varepsilon_{\rm ph}^{\rm co\prime}\xi(\theta),\ \ \varepsilon_m^{\rm UC\prime} = 2\gamma_m^2\varepsilon_{\rm ph}^{\rm co\prime}\xi(\theta),\ \ \varepsilon_{\rm cut}^{\rm UC\prime} = 2\gamma_m^2\varepsilon_{\rm cut}^{\rm co\prime}\xi(\theta), \tag{42}$$

and

$$\varepsilon_{\rm ph}^{\rm co\prime} = \frac{1+z}{2\Gamma_j}\varepsilon_{\rm ph}^{\rm co},\ \ \varepsilon_{\rm cut}^{\rm co\prime} = \frac{1+z}{2\Gamma_j}\varepsilon_{\rm cut}^{\rm co}. \tag{43}$$

The $\varepsilon F_\varepsilon$ peak energy of the UC emission is given by $\varepsilon_m^{\rm UC}$ in the case of $\beta \simeq -1$ and $p \simeq 3.2$.

In order to concentrate on the time-averaged spectrum including the high-latitude emission, we calculate the flux of the UC emission by neglecting the radial structure of the emitting shell for simplicity. In other words, we consider that the emission is produced instantaneously in the infinitely thin shell at $r = r_i$. This assumption gives us a model lightcurve that resembles the observed one. Then we obtain a formula for calculating the flux of the UC emission

$$F_\varepsilon(t) = \frac{3}{2}\tau F_{\varepsilon_{\rm ph}}^{\rm co}\xi(\theta(t))\frac{g(\varepsilon')}{[1+\Gamma_j^2\theta^2(t)]^2}, \tag{44}$$

where

$$\varepsilon' = (1+z)\varepsilon\frac{1+\Gamma_j^2\theta^2(t)}{2\Gamma_j} \tag{45}$$

$$\theta(t) = \sqrt{2}\left[1-\frac{c}{r_i}\left(\bar{t}_i - \frac{t}{1+z}\right)\right]^{1/2}, \tag{46}$$

and $\bar{t}_i$ is the emission time in the central engine frame (see Appendix A).

The peak energy and the peak flux of the UC emission are written as functions of the angle parameter $q(\theta) \equiv \Gamma_j^2\theta^2$:

$$\begin{aligned} \varepsilon_m^{\rm UC} &= 2\gamma_m^2\varepsilon_{\rm ph}^{\rm co}\frac{\xi(\theta)}{1+\Gamma_j^2\theta^2} \\ &\simeq 160\ {\rm MeV}\left[\frac{4q}{(1+q)^2}\right]\left(\frac{\gamma_m}{400}\right)^2\left(\frac{\varepsilon_{\rm ph}^{\rm co}}{1\ {\rm keV}}\right), \end{aligned} \tag{47}$$

$$\begin{aligned} \varepsilon_m^{\rm UC}F_{\varepsilon_m}^{\rm UC} &= 3\tau\gamma_m\gamma_c\varepsilon_{\rm ph}^{\rm co}F_{\varepsilon_{\rm ph}}^{\rm co}\frac{\xi^2(\theta)}{[1+\Gamma_j^2\theta^2]^3} \\ &\simeq 580\ {\rm keV\ cm^{-2}\ s^{-1}}\left[\frac{40q^2}{(1+q)^5}\right] \\ &\times\left(\frac{\tau}{4\times10^{-4}}\right)\left(\frac{\gamma_m}{400}\right)\left(\frac{\gamma_c}{400}\right)\left(\frac{\varepsilon_{\rm ph}^{\rm co}F_{\varepsilon_{\rm ph}}^{\rm co}}{30\ {\rm keVcm^{-2}s^{-1}}}\right), \end{aligned} \tag{48}$$

where the functions in the brackets [ ] both have values of zero at $q = 0$ and $q = \infty$ and have peaks of 1 at $q = 1$ and $\simeq 1.4$ at $q = 2/3$, respectively. This means that the UC flux has a peak at $q \simeq 1$, or $\theta \simeq \Gamma_j^{-1}$, i.e., the peak time of the UC emission lags behind that of the SSC emission on the angular spreading timescale, $\Delta t_i \simeq 2$ s. This is consistent with the observed lag of the GeV emission onset behind the MeV emission peak of the second pulse of GRB 080916C. Here the values of the jet parameters $\tau = 4\times10^{-4}$ and $\gamma_m = \gamma_c = 400$ are applicable for the 1st-order SSC emission of the jet being consistent with the observed MeV emission component (see § 3.2). This indicates that the UC emission of the electrons accelerated in the internal shock of the jet, emitting the observed MeV emission, can naturally explain the observed flux in the GeV range.

4. CONSTRAINTS ON MODEL PARAMETERS

In the above two sections we have shown that the upscattered cocoon emission model can explain the observed properties (ii) and (iii) of GRB 080916C listed in § 1. The high-energy lag of the second pulse (property (iii)) can be explained by the delayed peak time of the UC emission because of the anisotropic inverse Compton scattering. If the constraint on the cocoon physical parameters E_c and Γ_c (equation 5) is satisfied, the cocoon has not released its radiation when the first pulse is produced, and thus the first pulse is not accompanied by the UC emission (property (ii)). The observed high-energy spectrum of the first pulse $F_\varepsilon \propto \varepsilon^{-1.63\pm0.12}$ (Abdo et al. 2009) can be assumed to be produced only by the 1st-order SSC emission. This leads to an energy spectral index of the accelerated electrons $p \sim 3.2$ (see equation 32). The first and second internal shocks may have similar electron acceleration mechanisms, in which case we can take $p \sim 3.2$ also for the second MeV pulse.

In order to confirm whether this model can also explain the observed property (i), i.e., the combination of the 1st-order SSC and UC emission can reproduce the observed smooth power-law spectrum of the second pulse, we perform numerical calculations of the equation (44). We approximate the spectral shape as

$$g(\varepsilon') = \left(\frac{\varepsilon'}{\varepsilon_c^{\mathrm{UC}'}}\right)\left[1+\left(\frac{\varepsilon'}{\varepsilon_c^{\mathrm{UC}'}}\right)^s\right]^{\frac{-3/2}{s}} \times \left[1+\left(\frac{\varepsilon'}{\varepsilon_m^{\mathrm{UC}'}}\right)^s\right]^{\frac{\beta+(1/2)}{s}} \left[1+\left(\frac{\varepsilon'}{\varepsilon_{\mathrm{cut}}^{\mathrm{UC}'}}\right)^s\right]^{\frac{(-p/2)-\beta}{s}}, \quad (49)$$

where we adopt the value $s = 2$. We can also similarly calculate the spectrum of the SSC emission (see Appendix A), and combine the UC and SSC emission.

If the flux of the cocoon photospheric X-rays is given, i.e., E_c, Γ_c, r_*, and α are given, the fluxes of the UC and SSC emission of the jet are determined by the jet parameters $L, \Gamma_j, \Delta t_i, \epsilon_B$, and ϵ_e. Since $\Delta t_i \sim 2$ s is roughly given by the observations, and this value is necessary to explain the observed high-energy lag timescale, we have four free parameters. On the other hand, we have four characteristic observables; the peak fluxes and peak photon energies of the SSC component and the UC component. Therefore the jet parameters are expected to be constrained tightly.

Figure 2 shows the result of the time-averaged spectrum of the second pulse for the cocoon parameters

$$E_{c,52} = 1.0, \;\; \Gamma_c = 52, \;\; r_{*,11} = 2.5, \;\; \alpha = 0.05, \quad (50)$$

and $\beta = -1.2$. These values satisfy the constraints on the cocoon parameters, equations (5), (7), and (15). The *dashed line* represents the 1st-order SSC component plus the 2nd-order SSC component without taking account of Klein-Nishina effect, the *dot-dashed line* represents the cocoon X-ray emission, and the *dotted line* represents the UC component. The *thick solid line* is the combination of all the components taking into account the Klein-Nishina effect. The *thin solid line* and the *dot-short-dashed lines* represent the Band model spectrum fitted to the observed data and the 95% confidence errors, respectively (from the *Fermi* LAT/GBM analysis group, private communication). This figure shows that our model is roughly consistent with the observed spectrum at $\varepsilon \gtrsim 1$ MeV. Since the observed number flux of the second pulse at $\sim$ 1 GeV is $\sim$ 1 counts/s, the detection limit for $\varepsilon > 3$ GeV is roughly given by $\varepsilon F_{\varepsilon,\mathrm{lim}} \sim 10^3$ keV cm^{-2} s$^{-1}(\varepsilon/3$ GeV) (The effective area of the LAT detector is approximately constant for 1 GeV $\lesssim \varepsilon \lesssim$ 300 GeV, Atwood et al. 2009). Thus the small bump at $\sim$ 30 GeV cannot be detected. This is consistent with the non-detection of photons at $>$ 3 GeV. The adopted values of the jet parameters are

$$L_{55} = 1.1, \;\; \Gamma_{j,3} = 0.93, \;\; \Delta t_i = 2.3\,\mathrm{s}, \;\; \epsilon_B = 10^{-5}, \;\; \epsilon_e = 0.4, \quad (51)$$

and $p = 3.2$. The corresponding values of the optical depth for electron scattering and the characteristic electron Lorentz factors are

$$\tau = 3.5 \times 10^{-4}, \;\; \gamma_m = 400, \;\; \gamma_c = 390. \quad (52)$$

Figure 3 shows the results of the multi-band lightcurves for the same parameters. Each lightcurve is normalized to a peak flux of unity. This clearly displays the lag of the high-energy emission onset. We also plot the multi-band lightcurves averaged in 0.5 s time bins in Figure 4, which corresponds to the lightcurves measured by the GBM and LAT of *Fermi* satellite (Fig 1 of Abdo et al. 2009). The observed peak number flux of the GeV photons is only $\sim$ 1 counts/bin, so that the rising part of the GeV emission at $t \leq 5.5$ s could not be detected. This is consistent with the onset of the GeV emission being delayed behind that of the MeV emission.

5. DISCUSSION

5.1. *An additional emission component in the sub-MeV range?*

The 1st-order SSC emission and UC emission of the internal shock electrons of the jet can explain the main spectral peak (at $\varepsilon \sim 1$ MeV) and the delayed high-energy part (at $\varepsilon \gtrsim 100$ MeV), respectively, of the second pulse of GRB 080916C (see Figure 2). However, we should note a caveat for this model. The 1st-order SSC emission has a steep low-energy slope, i.e., $\varepsilon F_\varepsilon \propto \varepsilon^2$ at $\varepsilon < 1$ MeV because of strong synchrotron self-absorption effect (see equation 31), which is not consistent with the observed low-energy spectrum $\varepsilon F_\varepsilon \propto \varepsilon^{0.98\pm0.02}$ (Abdo et al. 2009). On the other hand, the 2nd-order SSC emission has the same steep low-energy slope, which is consistent with the non-detection of the spectral bump at $\varepsilon \gtrsim 1$ GeV. If there was no self-aborption effect, the 2nd-order SSC emission, even with the Klein-Nishina effect, would be so bright as to be detected (see also Wang et al. 2009). In order to reproduce the observed sub-MeV spectrum, we require an additional emission component, with careful consideration of the physical conditions of the emitting region. An additional sub-MeV emission produced by some process *near the emission region of the main MeV emission of the second pulse* would be up-scattered by the electrons emitting the MeV emission, like the SSC process without the self-absorption, and then the up-scattered flux would easily violate the observational upper limits.

Here we propose, for illustrative purposes, an additional sub-MeV emission whose up-scattered emission does not violate the observational limits. One can argue that additional sub-MeV emission may be produced in another internal shock (which we can call a “third internal shock") occurring far in front of the second internal shock shell at the same observed time. A fraction of the emission from the third internal shock propagates backward and is up-scattered by the second shell electrons into the high-energy range, but in this case, the electrons have cooled by the adiabatic expansion and then the up-scattered flux is expected to be dimmer than the case mentioned above.

Figure 5 demonstrates an example of such an additional sub-MeV emission. The *dashed line* is the same as the thick solid line in Figure 2, i.e., the time-averaged spectrum of the combination of the SSC and UC emission of the second internal shock and the cocoon X-ray emission. The *dotted line* represents the synchrotron emission of the third internal shock. Here we assume that this third, less energetic internal shock accelerates some fraction f of electrons with a power-law energy distribution (Bykov & Mészáros 1996; Eichler & Waxman 2005; Toma et al. 2008; Bosnjak et al. 2009) [7]. The adopted parameters are

$$L_{55} = 0.23,\ \ \Gamma_{j,3} = 1.8,\ \ \Delta t_i = 2.3 \text{ s},$$
$$\epsilon_B = 1.3 \times 10^{-3},\ \ \epsilon_e = 0.35,\ \ f = 3 \times 10^{-3}. \tag{53}$$

The corresponding values of the scattering optical depth for the accelerated electrons and the characteristic electron Lorentz factors are

$$\tau_{ac} = 8.2 \times 10^{-9},\ \ \gamma_m = 1.2 \times 10^5,\ \ \gamma_c = 5.6 \times 10^4. \tag{54}$$

The SSC emission of the third internal shock electrons are significantly suppressed by the Klein-Nishina effect. The cocoon X-rays and the optical synchrotron emission of the second internal shock are up-scattered by the third internal shock efficiently, whose fluxes have been taken into account for estimating γ_c. The former has the peak flux $\varepsilon F_\varepsilon \sim 200$ keV cm^2 s^{-1} at $\varepsilon \sim 10$ TeV. This may be absorbed by the extragalactic background radiation. The latter is shown by the *dot-dashed line* in Figure 5, which may arrive at the earth along with the second pulse in the high-energy range but be so dim as not to be detected by the LAT detector. The emission radius of the third shell is estimated by

$$r_{ia} \simeq 8.4 \times 10^{16} \text{ cm}. \tag{55}$$

Thus the radius where the backward photons from the third shell is up-scattered by the second shell is $\simeq (r_i + r_{ia})/2 \simeq 5.3 \times 10^{16}$ cm $\equiv R_{\rm ex} r_i$ where $R_{\rm ex} \simeq 2.4$. At this radius, the column density of the second shell is $R_{\rm ex}^2$ times smaller and the characteristic electrons Lorentz factors are $R_{\rm ex}$ times smaller because of the adiabatic expansion, so that the optical depth for the up-scattering is $R_{\rm ex}^4$ times smaller than that at $r = r_i$. The synchrotron emission from the third shell, up-scattered by the expanded second shell, is calculated by using equation (39) with $\xi = 1 - \cos(\pi - \theta')$, and the result is shown by the *thick dashed line* in Figure 5. This emission arrives at the earth $(R_{\rm ex} - 1)\Delta t_i \simeq 3.2$ s after the onset of the second pulse, and may not be detected by the LAT detector. The combined spectrum of the second internal shock emission (*dashed line*), the synchrotron emission of the third internal shock (*dotted line*), and the synchrotron emission of the second internal shock up-scattered by the third internal shock electrons (*dot-dashed line*) is shown by the *thick solid line* and it may be observed as the second pulse. This is consistent with the observed spectrum of the second pulse.

5.2. *Internal shock radius vs deceleration radius*

The jet material is finally decelerated by the interaction with the circumburst medium, into which the external shock propagates. Thus the internal shocks of the jet must occur below the deceleration radius of the first internal shock shell. The first shell is estimated to have the isotropic-equivalent kinetic energy $E \sim L\Delta t_i/(1+z) \simeq 4.7 \times 10^{54}$ erg and the bulk Lorentz factor $\Gamma_j \sim 10^3$ after the production of the first MeV pulse. The deceleration radius is then $r_{\rm dec} \simeq [17E/(16\pi\Gamma_j^2 n m_p c^2)]^{1/3} \sim 10^{17}$ cm $n^{-1/3}$. This would be larger than the internal shock radius r_i or r_{ia} if $n \lesssim 1$ cm^{-3}. This is in a reasonable range of typical values of the GRB circumburst medium density (Panaitescu & Kumar 2002; Yost et al. 2003). The deceleration time is estimated to be $t_{\rm dec} \simeq r_{\rm dec}(1+z)/(2c\Gamma_j^2) \sim 9\ n^{-1/3}$ s. After the UC emission ceases (i.e., $t > \Delta t_c + \Delta t_d \sim 15$ s) the high-energy emission may be due to the external shock (see Kumar & Barniol Duran 2009).

5.3. *Photospheric emission of the jet*

We have assumed that the jet is dominated by kinetic energy of baryons instead of magnetic energy. Zhang & Pe'er (2009) have argued that the non-detection of the photospheric thermal emission *of the jet* for GRB 080916C may exclude a possibility of a baryon-dominated jet and suggest that a Poynting-flux-dominated jet is preferred (see also Daigne & Mochkovitch 2002). They show that if the jet is dominated by thermal energy at $r = c\Delta t_i/(1+z) \simeq 2.8 \times 10^9\ (\Delta t_i/0.5 \text{ s})$ cm, the photospheric thermal emission of the jet is so bright that it can be detected, which is inconsistent with the observation. However, it is more reasonable that the jet has already accelerated up to a $\Gamma_j \approx 10^3$ before reaching that radius, through the usual adiabatic expansion starting from the central region of the progenitor star ($r_e \sim 10^6$ cm. This value corresponds to the gravitational radius of a black hole with a mass $M = 3M_\odot$). Thus the jet is dominated by kinetic energy at that radius, and the thermal emission of the jet may be much weaker than the estimate by Zhang & Pe'er (2009).

We assume that the jet is dominated by thermal energy at $r = r_e$, and it is accelerated by converting the thermal energy into kinetic energy. We can derive the flux of the residual thermal emission of the jet at the photosphere according to the standard fireball model, similar to that of the cocoon (see § 2). Let the initial bulk Lorentz factor of the jet at $r = r_e$ be $\Gamma_e \geq 1$. (It may be possible that a fraction of the black hole rotational energy is carried into the kinetic energy of the jet by the magnetic field.) Then the bulk Lorentz factor of the jet saturates at $r_{sj} = r_e\Gamma_j/\Gamma_e \simeq 10^9$ cm $r_{e,6}\Gamma_{j,3}\Gamma_e^{-1}$. The comoving number density of the jet shell $n' = L/(4\pi r^2 m_p c^3 \Gamma_j^2)$ and the Thomson optical depth $\tau = \sigma_T n' r/\Gamma_j = 1$ define the photospheric radius

$$r_{\rm phj} = \frac{\sigma_T L}{4\pi m_p c^3 \Gamma_j^3} \simeq 1.2 \times 10^{13} \text{ cm } L_{55}\Gamma_{j,3}^{-3}. \tag{56}$$

The comoving temperature of the jet shell evolves from $T_e' \simeq [L/(4\pi r_e^2 c \Gamma_e^2 a)]^{1/4}$ as $\propto r^{-1}$ at $r_e < r < r_{sj}$ and as $\propto r^{-2/3}$ at $r_{sj} < r < r_{\rm phj}$. Then we obtain the peak energy and the peak flux of the photospheric emission of the jet shell

$$\varepsilon_{\rm ph}^{\rm jet} \simeq 43 \text{ keV } L_{55}^{-5/12} r_{e,6}^{1/6} \Gamma_e^{-1/6} \Gamma_{j,3}^{8/3}, \tag{57}$$
$$\varepsilon_{\rm ph}^{\rm jet} F_{\varepsilon_{\rm ph}}^{\rm jet} \simeq 460 \text{ keV cm}^{-2} \text{ s}^{-1}\ L_{55}^{1/3} r_{e,6}^{2/3} \Gamma_e^{-2/3} \Gamma_{j,3}^{8/3}. \tag{58}$$

(The time-averaged flux is smaller by about a factor of 4.) This means that the photospheric thermal emission of the jet is marginally hidden by the prompt MeV emission (see Figure 5).

---

[7] We find it difficult to obtain an additional sub-MeV component by the SSC mechanism similar to the main MeV component. A sub-MeV component should be less energetic than the main MeV component, so that it should be $\gamma_m < \gamma_c$. In this case the flux at $\varepsilon_m^{\rm SC}$ should make a sub-MeV peak. Then $\varepsilon_m^{\rm SC}$ should be about one order of magnitude smaller than and $F_{\varepsilon_m}^{\rm SC}$ should be comparable with those for the main MeV component, and $\varepsilon_a/\varepsilon_m$ should be smaller than unity. However, such values may not be obtained by equation (28), (29) with $F_{\varepsilon_c}^{\rm SC} \rightarrow F_{\varepsilon_m}^{\rm SC}$ for $\gamma_m < \gamma_c$, and (31) with $\varepsilon_c \rightarrow \varepsilon_m$ and $\gamma_c \rightarrow \gamma_m$ for any reasonable set of the jet parameter values $\{L, \Gamma_j, \Delta t_i, \theta_p, \epsilon_B, \epsilon_e\}$.

The above analysis does not take account of possible effects from the stellar matter. The front of the jet is dissipated by the interaction with the stellar matter, and the shocked jet matter and the shocked stellar matter escape sideways to form the cocoon. The shocked jet matter in front of the clean jet at the break-out will make an X-ray flash. The brightness of the X-ray flash highly depends on the density profile of the star (Waxman & Mészáros 2003). We do not discuss this in further detail.

If re-conversion of jet kinetic energy into thermal energy due to interaction of the sides of the jet with the high-pressure cocoon is strong, the residual thermal emission may be brighter than the above estimate. The ratio of thermal energy to kinetic energy of the clean, adiabatically expanding jet shell at the stellar radius is $\simeq (r_*/r_{sj})^{-2/3} \sim 0.05$. Thus the re-conversion fraction at $r \leq r_*$ is required to be smaller than 5% to suppress the thermal flux down to the above estimate. However, many numerical simulations with various initial conditions of the jet and the star show that the re-conversion fractions can be much higher than 5% while the jet propagates in the star (e.g., Zhang et al. 2003; Mizuta et al. 2006; Morsony et al. 2007; Mizuta & Aloy 2009) and even well outside the star (Lazzati et al. 2009). This implies that the photospheric thermal emission of the jet for GRB 080916C may not be hidden by the SSC emission from the internal shock, being inconsistent with the observation.

It could be possible that the prompt MeV emission of GRB 080916C is mainly the photospheric emission of the jet (Mészáros & Rees 2000; Lazzati et al. 2009). In this case also, the delayed high-energy emission could be due to the up-scattering of the cocoon emission off the non-thermal electrons produced in internal shocks, where the SSC and synchrotron emission from the internal shocks are dimmer than the photospheric emission in the MeV energy range. This scenario requires different modeling from that in this paper.

Alternatively, as discussed by Zhang & Pe'er (2009), it is possible that the jet is initially dominated by magnetic energy and the baryons in the jet are accelerated by converting the magnetic energy into kinetic energy, so that the jet is dominated by the baryon kinetic energy at the internal shock radius (e.g., Vlahakis & Königl 2003; Komissarov et al. 2009; Lyubarsky 2009). The cocoon will be still produced by the shocked jet and shocked stellar matter, but a large fraction of the cocoon energy will be the magnetic energy. However, the magnetic fields could be tangled and dissipated through escaping from the jet into the cocoon and interacting with the shocked stellar matter and the ambient stellar envelope, so that the magnetic energy could become in equipartition to thermal (radiation) energy. The dynamics of such a cocoon after escaping from the star is similar to that in the non-magnetized jet case. This possibility is speculative, and magnetohydrodynamic simulations of the jet propagation in a star will be useful to address it. If this is true, our model based on the assumption that the MeV and high-energy emission components are produced by the 1st-order SSC radiation from the internal shocks and the up-scattered cocoon radiation, respectively, will be applicable. It is an open question how bright the photospheric thermal emission from the magnetized jet can be.

6. IMPLICATIONS FOR OTHER LONG AND SHORT GRBS

We have focused on the up-scattered cocoon emission for explaining the delayed high-energy emission of GRB 080916C. Since the delayed high-energy emission is observed for other bursts, it is useful to discuss whether the up-scattered cocoon emission may be important for other bursts.

Our model involves many parameters; the cocoon parameters E_c, Γ_c, r_*, and α, and the jet parameters L, θ_j, Γ_j, Δt_i, ϵ_B, and ϵ_e. The cocoon parameters depend significantly on the luminosity and the initial opening angle of the jet and the density profile of the progenitor star (e.g., Mészáros & Rees 2001; Morsony et al. 2007), so that their values for general bursts are unclear. Here, for simplicity, we fix the values of the cocoon parameters as those adopted above for GRB 080916C.

For further simplicity, we only consider the bursts for which the prompt emission in the soft γ-ray band could be produced by the 1st-order SSC radiation of the electrons. Indeed, it seems difficult to explain the prompt emission of *all* GRBs in the simple SSC model (Piran et al. 2009; Kumar & Narayan 2009). The jet parameters for typical long GRBs are inferred from various observations; $L \simeq 10^{53}$ erg s^{-1}, $\theta_j \simeq 0.1$ (Ghirlanda et al. 2004), and $\Gamma_j \simeq 300$ (e.g., Lithwick & Sari 2001; Molinari et al. 2007). The other parameters with values similar to those adopted for GRB 080916C in this paper, i.e., $\Delta t_i/(1+z) \simeq 0.4$ s, $\epsilon_B \simeq 10^{-5}$, and $\epsilon_e \simeq 0.2$ may provide $\gamma_c \sim \gamma_m$ and account for the spectral peak energy $\varepsilon_m^{\rm SC} \sim 200$ keV and spectral peak flux $\varepsilon_m^{\rm SC} F_{\varepsilon_m}^{\rm SC} \sim 100$ keV cm^{-2} s^{-1} of typical long GRBs with redshifts $z \simeq 2$ in the SSC model (see § 3.2).

In this case we have the value of $\tau\gamma_m\gamma_c$ similar to that for GRB 080916C, so that the up-scattered cocoon emission could be important for those bursts (see equation 48), although we require to study some kinematic effects carefully. Now we have

$$\Gamma_c \theta_j \simeq 5 > 1, \tag{59}$$

so that the de-beaming effect of the relativistic motion of the cocoon shell for the seed photons of the UC emission is significant. However, this effect may be cancelled out by the beaming effect of the relativistic motion of the jet. The internal shock radius is $r_i \simeq 2 \times 10^{15}$ cm, which is still much larger than the photospheric radius of the cocoon $r_{\rm ph} \simeq 2 \times 10^{14}$ cm. Then we have the angle between the direction of the photon beam and the expansion direction of the scattering point of the jet in the lab frame $\chi \approx (r_{\rm ph}/r_i)(\theta_j - \theta) \sim 10^{-2}$ (see Figure 1) and

$$\Gamma_j \chi \sim 3 > 1. \tag{60}$$

Since $\Gamma_c \theta_j \sim \Gamma_j \chi$, the de-beaming and beaming effects may compensate each other, so that the seed radiation can have the flux and spectrum similar to those for GRB 080916C. Therefore it is quite possible that the up-scattered cocoon emission contributes to typical long GRBs and they account for the delayed high-energy emission.

The condition $\Gamma_j \chi > 1$ means that $\chi > \theta$ (since we focus on the region of $\theta \sim \Gamma_j^{-1}$) and $\xi \approx 2/(1+\Gamma_j^2\theta^2)$. Then these bursts will not have the high-energy lags, i.e., the property (iii) (see equation 48). Since the seed cocoon photons come from the front in the jet frame, the UC emission in the observer frame is stronger from the line of sight.

For bursts with smaller $\Delta t_i/(1+z)$ so that $r_i \lesssim r_{\rm ph}$, the delay timescale of the up-scattered cocoon emission behind the onset of the internal shock emission should be on the order of $(1+z) r_{\rm ph} \theta_j / c \sim 10^3$ s, and thus in this case, the up-scattering effect may be important only if the duration of the prompt emission is longer than $\sim 10^3$ s.

Some short GRBs might originate from the collapses of the massive stars (Janiuk & Proga 2008; Zhang et al. 2009; Toma et al. 2005), and thus they could have the delayed UC emission. Even if other short GRBs are produced by the compact star mergers, it might be possible that the jet is accompanied by the delayed disc wind (Metzger et al. 2008) and that the emission from the disc wind is up-scattered by the electrons accelerated in the jet. For either progenitor models, the delayed high-energy emission associated with short GRBs, if any, would provide an interesting tool to approach their origins.

7. SUMMARY AND FURTHER IMPLICATIONS

The *Fermi* satellite provides an unparalleled broad energy coverage with good temporal resolution, and it is accumulating a steady stream of new data on the high-energy emission of GRBs. GRB 080916C, detected by *Fermi*, showed unexpected properties in the high-energy range, i.e., > 100 MeV, which are listed in § 1. These include the new results on prompt emission; (i) the time-resolved high-energy spectra are described by smooth power-laws up to a photon with energy ≈ 13.2 GeV, (ii) the high-energy emission is not detected with the first MeV pulse (i.e., the first pulse in the $\lesssim 1$ MeV range) and begins to be detected along with the second MeV pulse, (iii) the second pulse has the later peaks in the higher energy bands, and (iv) the high-energy emission lasts at least 1400 s, much longer than the duration of the MeV emission. We have discussed a model in which the prompt emission spectrum consists of an MeV component produced by the SSC emission of electrons accelerated in internal shocks in the jet and the high-energy component produced by up-scattering of the cocoon X-rays off the same electrons, and we have shown that this model can explain the above three observed properties (i), (ii), and (iii). The expanding cocoon may become optically thin some time later than the first internal shock of the jet (equation 4), so that the first MeV pulse may not be associated with the up-scattered cocoon (UC) emission while the second MeV pulse may be associated with it (property (ii), see § 2). The UC emission has an anisotropic energy distribution in the comoving frame of the jet so that the observed UC emission is stronger from the higher-latitude region of the shell. This results in the lag of the flux peak of the UC emission behind the MeV emission onset on the angular spreading timescale (property(iii), see § 3, Figure 3, and 4). Figure 2 shows that the combination of the SSC and UC emission can reproduce the observed high-energy spectral data (property (i), see § 4). The UC emission is short-lived and may not account for the whole high-energy emission which lasts longer than the MeV emission (property (iv)). It is natural that the high-energy emission in the later times is related to the afterglow. This has been shown by Kumar & Barniol Duran (2009). However, the early portion of the high-energy emission should be the UC emission, because the external shock cannot reproduce the observed steep rise of the flux.

The observed flux and width of the second pulse of this burst indicate that the isotropic-equivalent luminosity of the jet $L \simeq 10^{55}$ erg s^{-1} and the angular spreading timescale of the pulse $\Delta t_i \simeq 2$ s. The absence of a $\gamma\gamma$ absorption cutoff in the spectra leads to a jet bulk Lorentz factor of $\Gamma_j \simeq 10^3$ (Abdo et al. 2009) (see also Aoi et al. 2009). (A larger Γ_j would make the internal shock radius larger than the deceleration radius of the shell.) Then in the internal shock model with a mean random Lorentz factor of the shocked protons $\theta_p \lesssim 8$ (and all of the electrons being accelerated, i.e., $f = 1$), the spectral peak flux at the MeV energy cannot be produced by synchrotron emission (see equation 26), but can be produced by the 1st-order SSC emission of the electrons. The observed peak energy and the peak flux of the MeV emission constrains the 1st-order SSC emission mechanism requiring the microphysical parameters as $\epsilon_B \simeq 10^{-5} \ll \epsilon_e \simeq 0.4$, or $\gamma_m \sim \gamma_c \sim 400$. These parameters naturally make the UC emission of the same electrons compatible with the observed flux at the GeV energy, and $\Delta t_i \simeq 2$ s is consistent with the observed lag of the GeV emission behind the onset of the MeV emission.

In our model, we expect this burst to have had bright synchrotron emission in the optical band, like the "naked-eye" GRB 080319B (Racusin et al. 2008). The 1st-order SSC emission peaking at the MeV energy has a steep slope in the lower energy range because of a strong synchrotron self absorption effect (see Figure 2). This effect, along with the Klein-Nishina effect, suppresses the 2nd-order SSC emission so it is not detected in the $\varepsilon > 1$ GeV range. On the other hand, an additional emission component is required to reproduce the observed spectrum in the sub-MeV energy range. We propose that another internal shock with the smaller luminosity $L \simeq 2 \times 10^{54}$ erg s^{-1} and a fraction of electrons accelerated $f \simeq 3 \times 10^{-3}$ may produce the sub-MeV emission (see § 5.1 and Figure 5). This interpretation is somewhat ad hoc but plausible, and we argue that it is compatible with the *Fermi* observation.

Many numerical simulations suggest that the hydrodynamical jet will store a large fraction of thermal energy because of the interaction of the jet with the high-pressure cocoon (Morsony et al. 2007; Lazzati et al. 2009). Then the jet will emit a bright photospheric thermal radiation, which is not observed for GRB 080916C (Zhang & Pe'er 2009). It could be possible that the prompt MeV emission is mainly the photospheric emission of the jet (instead of the 1st-order SSC radiation from the internal shocks), while the high-energy emission component is still due to the up-scattered cocoon emission from the internal shocks. Alternatively, the jet of GRB 080916C may be initially dominated by magnetic energy. It is not clear yet whether a large fraction of thermal energy will be stored in the magnetized jet while it propagates in a star. The jet could become dominated by baryon kinetic energy at large radius, and the cocoon dynamics could be similar to that in the non-magnetized jet case, so that our model in this paper would be entirely applicable (see § 5.3).

GRB 080916C is the only burst for which the observational data is extensive enough and the analysis is fairly complete at the moment, so that we have focused on this GRB to discuss our model in detail. Since our model involves much information from the observational data and many parameters, it is not easy to perform a more general study of the UC emission at this stage. However our model is generic, and we have briefly shown that it could apply to other *Fermi*-LAT GRBs with typical parameters $L \simeq 10^{53}$ erg s^{-1}, $\theta_j \simeq 0.1$, and $\Gamma_j \simeq 300$ for which the prompt emission in the soft γ-ray range is produced by the 1st-order SSC radiation of electrons (see § 6). We may do a comprehensive study of our model when more *Fermi*-LAT GRBs are analyzed. The up-scattering effect could apply to short GRBs as well. Investigating the seed photons for the delayed high-energy emission of short GRBs would be an interesting approach to their origins.

A simple prediction of our model is that prompt emission spectra of at least some long GRBs would have an excess above the Band spectrum around ~ 1 keV due to the cocoon photospheric emission, and this excess should have a different temporal behavior from that of the MeV emission. Since the *Swift* XRT detector can observe the GRB prompt emission in the $0.3-10$ keV range at least 100 s after the triggers, the cocoon X-ray emission could in principle be observed if its onset times are $t_{\rm on} > 100$ s. In this case, we could examine the up-scattering effect of the cocoon emission if $t_{\rm on}$ is smaller than the burst duration T, while the cocoon emission may contribute to the early X-ray afterglow if $t_{\rm on} \gtrsim T$ (Pe'er et al. 2006). For long GRBs with $t_{\rm on} < 100$ s, the up-scattering effect could be tested by future satellite, e.g., *EXIST* [8], which is designed to have a soft X-ray detector and a good triggering capability.

If our model is correct, we can constrain the parameter range for which hadronic effects are important on the high-energy emission of GRBs, and we can also constrain the models of high-energy cosmic ray acceleration. Also, the delay time of the onset of the high-energy emission, $t_{\rm on}$, is directly linked to the optical-thinning time of the expanding cocoon, which constrains the physical parameters of the progenitor star and the cocoon material of GRBs. For GRB 080916C, the stellar radius r_* and the total energy E_c and mass M_c of the cocoon are constrained to be $0.3 < E_{c.52}^{-2}(M_c/10^{-4}M_\odot)^{2.5} \lesssim 0.9$ and $r_{*,11} \gtrsim 0.8\ E_{c,52}^{5}(M_c/10^{-4}M_\odot)^{-3}$ (see equations 5 and 15). The cocoon energy and the cocoon mass come from the jet energy released within the star and the stellar mass swept by the jet, respectively. These constraints therefore provide potential tools for investigating the structure of the progenitor star just before the explosion, as well as the physical conditions of the jet propagating inside the stellar envelope through either analytical (e.g., Mészáros & Rees 2001; Matzer 2003; Toma et al. 2007) or numerical (e.g., Zhang et al. 2003; Mizuta et al. 2006; Morsony et al. 2007) approaches.

We thank K. Murase and the *Fermi* LAT/GBM group members (especially F. Piron and V. Connaughton, who provided the Band model spectrum fitted to the observed data with errors) for useful discussions. We are grateful to the referee, D. Lazzati, for several important comments, and to Y. Z. Fan, S. Inoue, K. Ioka, T. Nakamura, R. Yamazaki, and B. Zhang for useful discussions after the submission of this paper. We acknowledge NASA NNX09AT72G, NASA NNX08AL40G, and NSF PHY-0757155 for partial support. XFW was supported by the National Natural Science Foundation of China (grants 10503012, 10621303, and 10633040), National Basic Research Program of China (973 Program 2009CB824800), and the Special Foundation for the Authors of National Excellent Doctorial Dissertations of P. R. China by Chinese Academy of Sicences.

---

[8] http://exist.gsfc.nasa.gov

REFERENCES

Abdo, A. A., and the Fermi LAT and Fermi GBM Collaborations 2009, Science, 323, 1688
Ahanorian, F. A., & Atoyan, A. M. 1981, Ap&SS, 79, 321
Aoi, J., Murase, K., Takahashi, K., Ioka, K., & Nagataki, S. 2009, submitted to ApJ (arXiv:0904.4878)
Asano, K., Inoue, S., & Mészáros, P. 2009, ApJ, 699, 953
Atwood, W. B., et al. 2009, ApJ, 697, 1071
Band, D. L., et al. 1993, ApJ, 413, 281
Beloborodov, A. M. 2005, ApJ, 618, L13
Bosnjak, Z., Daigne, F., & Dubus, G. 2009, A&A, 498, 677
Brunetti, G. 2001, Astropart. Phys., 13, 107
Bykov, A. M., & Mészáros, P. 1996, ApJ, 1996, 461, L37
Daigne, F., & Mochkovitch, R. 2002, MNRAS, 336, 1271
Dermer, C. D. 2002, ApJ, 2002, 574, 65
Dermer, C. D. 2004, ApJ, 614, 284
Eichler, D., & Waxman, E. 2005, ApJ, 627, 861
Falcone, A. D., et al. 2008, GRB section of the white paper on the status and future of ground-based TeV gamma-ray astronomy (arXiv:0810.0520)
Fan Y. Z., Piran, T., Narayan, R., & Wei, D. M. 2008, MNRAS, 384, 1483
Fan, Y. Z. 2009, MNRAS, 397, 1539
Ghirlanda, G., Ghisellini, G., & Lazzati, D. 2004, ApJ, 616, 331
Granot, J., Piran, T., & Sari, R. 1999, ApJ, 513, 679
Greiner, J., et al. 2009, A&A, 498, 89
Guetta, D., & Granot, J. 2003, ApJ, 585, 885
Gupta, N., & Zhang, B. 2007, MNRAS, 380, 78
Ioka, K., & Nakamura, T. 2001, ApJ, 554, L163
Janiuk, A., & Proga, D. 2008, ApJ, 675, 519
Komissarov, S. S., Vlahakis, N., Königl, A., & Barkov, M. V. 2009, MNRAS, 394, 1182
Kumar, P., & McMahon, E. 2008, ApJ, 384, 33
Kumar, P., & Narayan, R. 2009, MNRAS, 395, 472
Kumar, P.. & Barniol Duran, R. 2009, arXiv:0905.2417
Lazzati, D., Morsony, B., & Begelman, M. 2009, ApJ, 700, L47
Li, Z. 2009, submitted to ApJ (arXiv:0810.2932)
Lithwick, Y., & Sari, R. 2001, ApJ, 555, 540
Lyubarsky, Y. 2009, ApJ, 698, 1570
Matsumiya, M., & Ioka, K. 2003, ApJ, 595, L25
Matzner, C. D. 2003, MNRAS, 345, 575
Mészáros, P., Laguna, P., & Rees, M. J. 1993, ApJ, 415, 181
Mészáros, P., & Rees, M. J. 2000, ApJ, 530, 292
Mészáros, P., & Rees, M. J. 2001, ApJ, 556, L37
Mészáros, P. 2006, Rep. Prog. Phys., 69, 2259
Metzger, B. D., Piro, A. L., & Quataert, E. 2008, MNRAS, 390, 781
Mizuta, A., Yamazaki, T., Nagataki, S., & Mineshige, S. 2006, ApJ, 651, 960
Mizuta, A., & Aloy, M. A. 2009, ApJ, 699, 1261
Molinari, E., et al. 2007, A&A, 469, L13
Morsony, B. J., Lazzati, D., & Begelman, M. C. 2007, ApJ, 665, 569
Panaitescu, A., & Mészáros, P. 2000, ApJ, 544, L17
Panaitescu, A., & Kumar, P. 2002, ApJ, 571, 779
Pe'er, A., Mészáros, P., & Rees, M. J. 2006, ApJ, 652, 482
Piran, T., Shemi, A., & Narayan, R. 1993, MNRAS, 263, 861
Piran, T., Sari, R., & Zou, Y. C. 2009, MNRAS, 393, 1107
Racusin, J. L., et al. 2008, Nature, 455, 183
Ramirez-Ruiz, E., Celloti, A., & Rees, M. J. 2002, MNRAS, 337, 1349
Rees, M. J., & Mészáros, P. 1994, ApJ, 430, L93
Rees, M. J., & Mészáros, P. 2005, ApJ, 628, 847
Sari, R., & Esin, A. A. 2001, ApJ, 548, 787
Toma, K., Yamazaki, R., & Nakamura, T. 2005, ApJ, 620, 835
Toma, K., Ioka, K., Sakamoto, T., & Nakamura, T. 2007, ApJ, 659, 1420
Toma, K., Ioka, K., & Nakamura, T. 2008, ApJ, 673, L123
Vlahakis, N., & Königl, A. 2003, ApJ, 596, 1104
Wang, X. Y., & Mészáros, P. 2006, ApJ, 643, L95
Wang, X. Y., Li, Z., Dai, Z. G., & Mészáros, P. 2009, ApJ, 698, L98
Waxman, E., & Mészáros, P. 2003, ApJ, 584, 390
Woods, E., & Loeb, A. 1999, ApJ, 523, 187
Yamazaki, R., Ioka, K., & Nakamura, T. 2003, ApJ, 593, 941
Yost, S. A., Harrison, F. A., Sari, R., & Frail, D. A. 2003, ApJ, 597, 459
Zhang, B., et al. 2006, ApJ, 642, 354
Zhang, B. 2007, Chin. J. Astron. Astrophys., 7, 1
Zhang, B., & Pe'er, A. 2009, ApJ, 700, L65
Zhang, B., et al. 2009, ApJ, 703, 1696
Zhang, W., Woosley, S., & MacFadyen, A. I. 2003, ApJ, 586, 356
Zou, Y. C., Fan, Y. Z., & Piran, T. 2009, MNRAS, 396, 1163

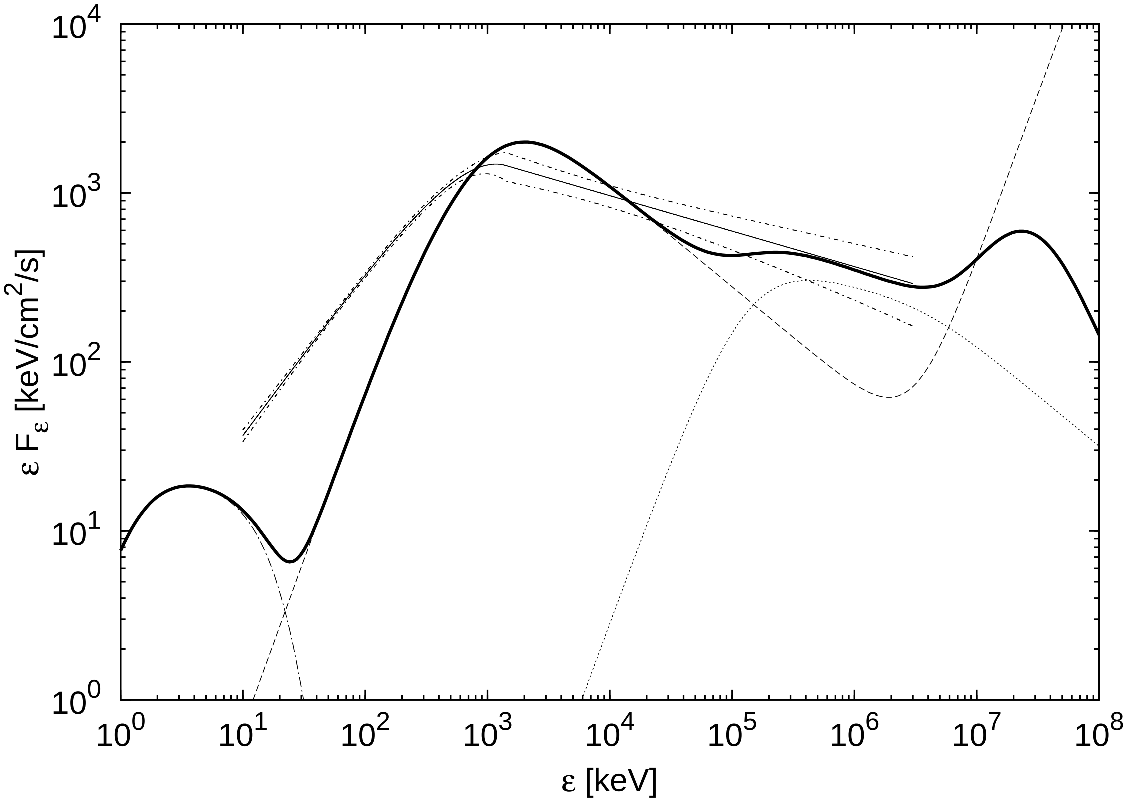

FIG. 2.— Time-averaged spectrum of the second pulse calculated in the up-scattered cocoon emission model. The 1st-order SSC component plus 2nd-order SSC component without including the Klein-Nishina effect (*dashed line*), the cocoon photospheric emission (*dot-dashed line*), and the up-scattered cocoon (UC) emission (*dotted line*) are shown. The *thick solid line* represents the combination of these, taking account of the Klein-Nishina effect, which is roughly consistent, at $\varepsilon \gtrsim 1$ MeV, with the Band model spectrum (*thin solid line*) with 95% confidence errors (*dot-short-dashed lines*) (from the LAT/GBM group of *Fermi*). The bump at ~ 30 GeV is so dim as not to be detected. The adopted parameters are listed in equation (50) and (51).

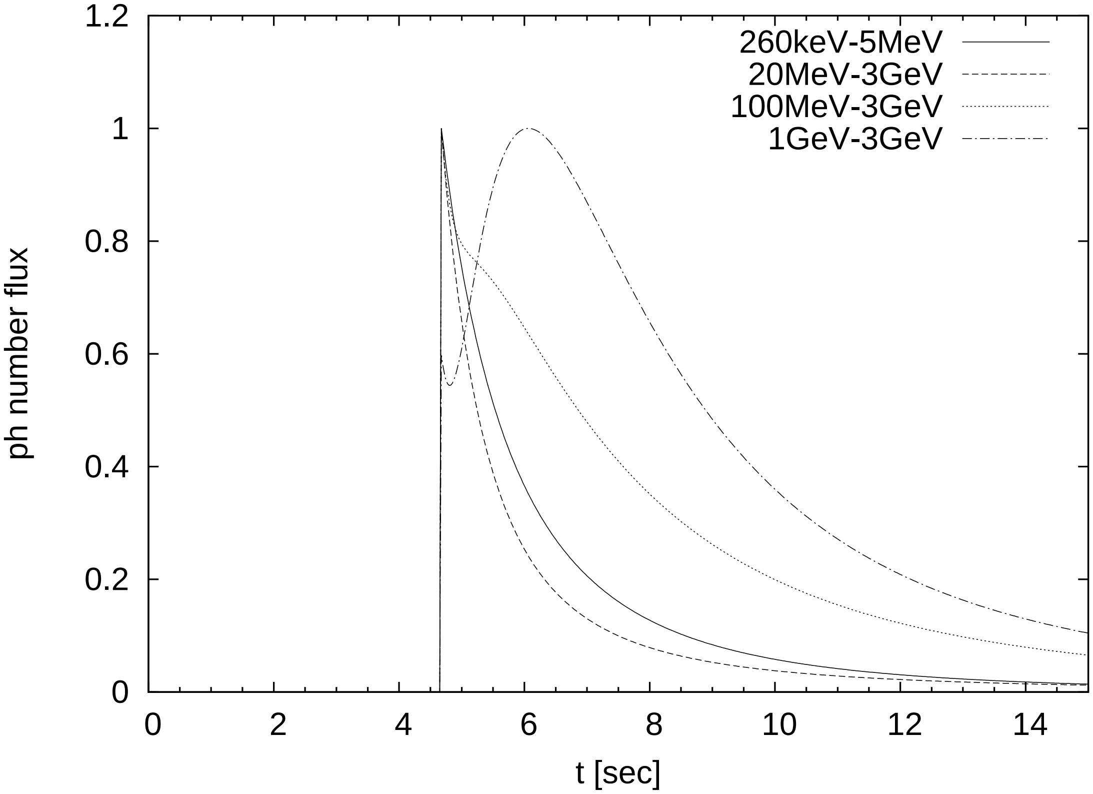

FIG. 3.— Photon number fluxes in several frequency ranges calculated in the up-scattered cocoon emission model. Time resolution is set to be 25 ms. Each lightcurve is normalized to a peak flux of unity. The peak of the GeV lightcurve is delayed behind that of the MeV lightcurve.

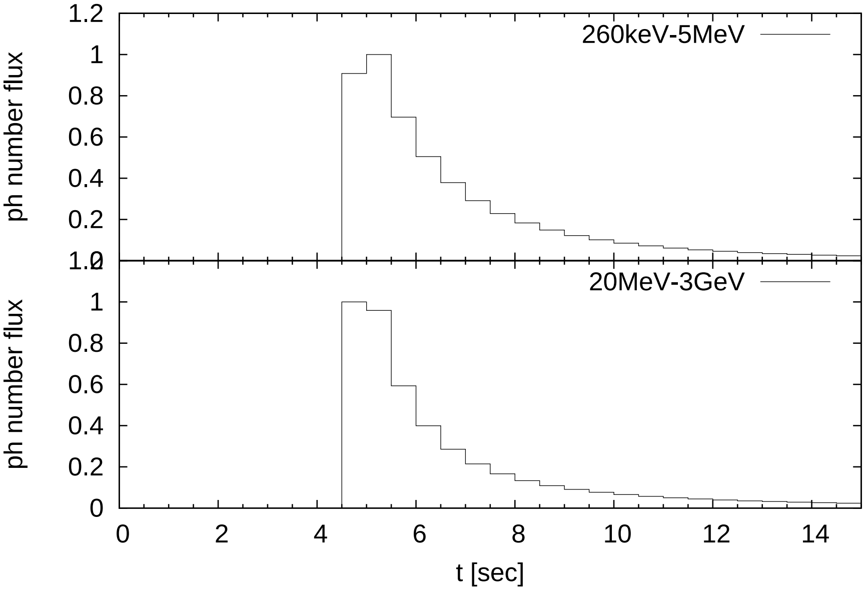

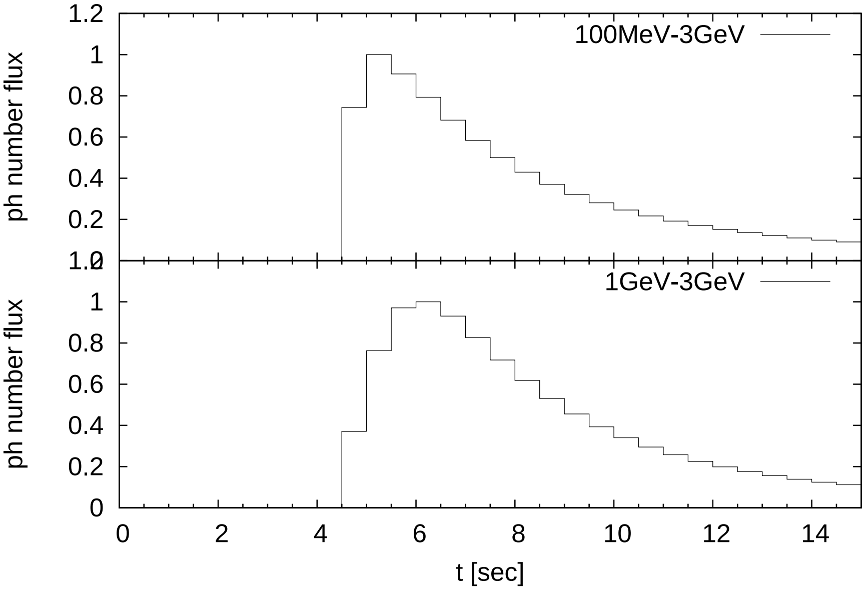

FIG. 4.— Same as Figure 3, but integrated in 0.5 s time bins. The observed number flux of the GeV photons is only ~ 1 counts/bin (Abdo et al. 2009), so that only the delayed peak at 5.5 s $\lesssim t \lesssim 7$ s could be detected.

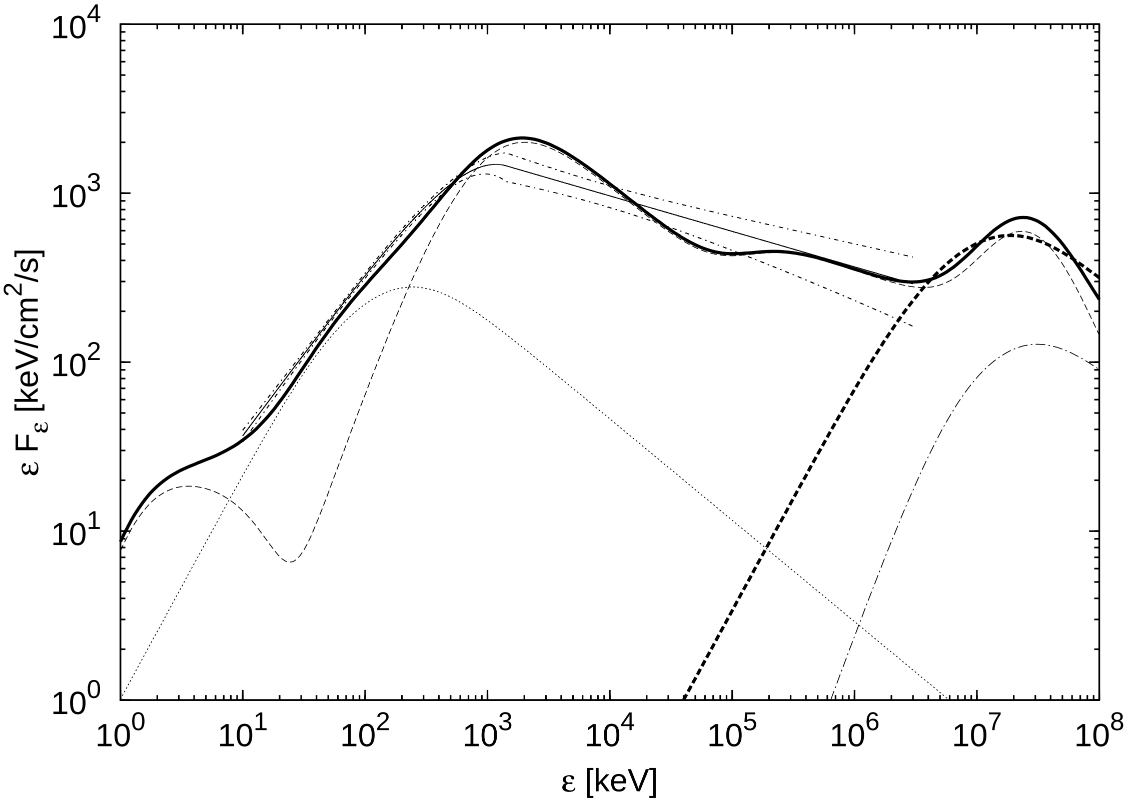

FIG. 5.— Combined time-averaged emission spectrum of the second and third internal shocks and the cocoon. The *dashed line* is the same as the thick solid line in Figure 2, i.e., the cocoon X-rays + the SSC and up-scattered cocoon (UC) emission of the second internal shock of the jet. A third less-energetic internal shock occurring at the same observer time as the second internal shock but far in front of it produces synchrotron emission (*dotted line*), and this emission is up-scattered into the GeV range by the second internal shock shell, arriving at the earth $\simeq 3.2$ s after the onset of the second pulse (*thick dashed line*). The optical synchrotron emission from the second internal shock, up-scattered by the third internal shock electrons, is shown by the *dot-dashed line*. The combined spectrum of the components arriving as the second pulse, i.e., the dashed line + the dotted line + the dot-dashed line, is represented by the *thick solid line* and it is consistent with the Band model spectrum (*thin solid line*) with 95% confidence errors (*dot-short-dashed lines*) (from the LAT/GBM group of *Fermi*). The bump at ~ 30 GeV is so dim as not to be detected. The adopted parameters of the third internal shock are listed in equation (53).

APPENDIX

FLUX OF INSTANTANEOUS EMISSION FROM THIN SHELL

We can calculate the observed specific flux from the shell expanding toward us relativistically by (Granot et al. 1999; Woods & Loeb 1999)

$$F_\varepsilon(t) = \frac{1+z}{d_L^2}\int d\phi \int d(\cos\theta)\int dr r^2 \frac{j'_{\varepsilon'}(\mathbf{r},\bar{t})}{\Gamma_j^2(1-\beta_j\cos\theta)^2}, \tag{A1}$$

where $\varepsilon' = (1+z)\varepsilon\Gamma_j(1-\beta_j\cos\theta)$ and $t = (1+z)[\bar{t}-(r/c)\cos\theta]$. For the instantaneous emission from the infinitely thin shell, the comoving emissivity can be approximated by (see also Ioka & Nakamura 2001; Yamazaki et al. 2003; Dermer 2004)

$$j'_{\varepsilon'}(\mathbf{r},\bar{t}) \to j'_{\varepsilon'}\Delta t'\Delta r'\delta(\bar{t}-\bar{t}_i)\delta(r-r_i), \tag{A2}$$

where $\Delta t' = r_i/c\Gamma_j$ and $\Delta r' = r_i/\Gamma_j$ are the comoving dynamical timescale and the comoving width of the shell. The delta functions represent the approximation of the instantaneous emission at $\bar{t} = \bar{t}_i$ in the infinitely thin shell at $r = r_i$. The integration can be performed straightforwardly as

$$F_\varepsilon(t) = F_\varepsilon(t_0)\frac{1}{[1+\Gamma_j^2\theta^2(t)]^2}, \tag{A3}$$

where

$$F_\varepsilon(t_0) = \frac{1+z}{d_L^2}8\pi r_i^3 j'_{\varepsilon'} \tag{A4}$$

$$\varepsilon' = (1+z)\varepsilon\frac{1+\Gamma_j^2\theta^2(t)}{2\Gamma_j} \tag{A5}$$

$$\theta(t) = \sqrt{2}\left[1-\frac{c}{r_i}\left(\bar{t}_i-\frac{t}{1+z}\right)\right]^{1/2}. \tag{A6}$$

For the up-scattered cocoon emission, $j'_{\varepsilon'}$ is given by equation (39) and this leads to equation (44).

For the 1st-order SSC emission, the comoving emissivity is given by

$$j'_{\varepsilon'} = \tau\frac{\sqrt{3}e^3B'n'}{4\pi m_e c^2}f(\varepsilon'), \tag{A7}$$

where

$$f(\varepsilon') = \begin{cases} \left(\frac{\varepsilon_a^{\mathrm{SC}\prime}}{\varepsilon_c^{\mathrm{SC}\prime}}\right)^{1/3}\left(\frac{\varepsilon'}{\varepsilon_a^{\mathrm{SC}\prime}}\right)^{1}, & \text{for } \varepsilon' < \varepsilon_a^{\mathrm{SC}\prime}, \\ \left(\frac{\varepsilon'}{\varepsilon_c^{\mathrm{SC}\prime}}\right)^{1/3}, & \text{for } \varepsilon_a^{\mathrm{SC}\prime} < \varepsilon' < \varepsilon_c^{\mathrm{SC}\prime}, \\ \left(\frac{\varepsilon'}{\varepsilon_c^{\mathrm{SC}\prime}}\right)^{-1/2}, & \text{for } \varepsilon_c^{\mathrm{SC}\prime} < \varepsilon' < \varepsilon_m^{\mathrm{SC}\prime}, \\ \left(\frac{\varepsilon_m^{\mathrm{SC}\prime}}{\varepsilon_c^{\mathrm{SC}\prime}}\right)^{-1/2}\left(\frac{\varepsilon'}{\varepsilon_m^{\mathrm{SC}\prime}}\right)^{-p/2}, & \text{for } \varepsilon_m^{\mathrm{SC}\prime} < \varepsilon', \end{cases} \tag{A8}$$

and

$$\varepsilon_a^{\mathrm{SC}\prime} = \frac{1+z}{2\Gamma_j}\varepsilon_a^{\mathrm{SC}},\quad \varepsilon_c^{\mathrm{SC}\prime} = \frac{1+z}{2\Gamma_j}\varepsilon_c^{\mathrm{SC}},\quad \varepsilon_m^{\mathrm{SC}\prime} = \frac{1+z}{2\Gamma_j}\varepsilon_m^{\mathrm{SC}}. \tag{A9}$$

This leads to

$$F_\varepsilon(t) = \tau F_{\varepsilon_c}\frac{f(\nu')}{[1+\Gamma_j^2\theta^2(t)]^2}. \tag{A10}$$